Transmitter Impedance Characteristics for Airborne Spectrum Signature

William B. Henry, Wilbur R. DeHart
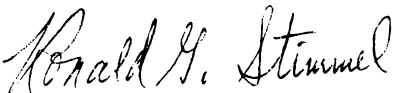
and Joseph E. Ferris

FOREWORD

This report, 7956-1-F, was prepared by The University of Michigan
Radiation Laboratory, Department of Electrical Engineering, under
the direction of Professor Ralph E. Hiatt on Air Force Contract
AF 33(615)-3454, Project 4357 "Transmitter Impedance Characteristics
for Airborne Spectrum Signature." The work was administered under
the direction of the Air Force Avionics Laboratory, Wright-Patterson
AFB, Ohio. The Task Engineer was Mr. Kenneth W. Tomlinson and the
Project Engineer was Mr. H. Bartman.

This report covers the period 1 April 1966 through 30 January 1968.

This report was submitted by the authors 20 February 1968.

This technical report has been reviewed and is approved.

JOSEPH A. DOMBROWSKI
Lt Colonel, USAF
Chief, Electronic Warfare Division

ABSTRACT

The problem of predicting airborne spectrum signatures is divided into three sections:

1) The transmitter spectrum signatures,

2) The effect of the transmission line, and

3) The radiation characteristics of the antenna and airframe.

This report is concerned with the first two of these sections, the third having been studied on a predecessor contract (Ferris, et al, 1966). Transmission lines are studied first. Expressions for the power transfer through a lossy transmission line as a function of line length, loss, and antenna and transmitter VSWR are developed. The results are valid for single mode systems.

After the power transfer expressions are developed, the transmitter behavior is studied. It has been found that the level of the harmonics generated is somehow related to the impedance of the termination at the fundamental frequency. These results are presented graphically in the form of "harmonic" Rieke diagrams. Finally, models to predict this behavior are introduced. No adequate model has been developed but neither has the last proposed model been discarded. More work in this area is indicated before the transmitter behavior can be accurately predicted.

ACKNOWLEDGEMENT

TABLE OF CONTENTS

LIST OF ILLUSTRATIONS

List of Illustrations, continued.

NOMENCLATURE

i_b instantaneous plate current

I_b average (DC) plate current

$\left| \hat{I}_p \right|_n$ magnitude of the n'th component of plate current

e_b total instantaneous plate voltage

E_b average (DC) plate voltage

E_{bb} plate supply voltage

$\left| \hat{E}_p \right|_n$ magnitude of the n'th component of plate voltage

e_c total instantaneous grid voltage

E_c average (DC) grid voltage

E_{cc} grid supply voltage

$\left| \hat{E}_g \right|_n$ magnitude of the n'th component of grid voltage

i_c total instantaneous grid current

I_c average (DC) grid current

$\left| \hat{I}_g \right|_n$ magnitude of the n'th component of grid voltage

I

INTRODUCTION

The general radio frequency interference (RFI) prediction problem can be stated quite simply as, "What is the chance that radio frequency electromagnetic radiations will interfere with the successful operation of a given system?". Without attempting to define "interfere" or "successful operation", we note that in order to answer the question we require two sets of input data:

1)   The susceptibility of a particular system to interference by radiations of a specific frequency, intensity, and mode; and

2)   The probability that radiated energy of a given frequency, intensity, and mode will be incident at the system.

Restricting our consideration to signals emitted by "transmitters" and received by "receivers", the problem can be diagrammed as in Fig. 1-1. Only one input to the receiving system is shown. There will be in general n inputs from n different transmitting systems similar to the one diagrammed. The University of Michigan has been engaged in a series of contracts with the Air Force to investigate methods for improving RFI predictions by determining the radiated spatial and spectral energy densities from certain classes of generators and radiators. More specifically, the question of concern has been, "How can one best predict the radio frequency energy radiated from an airborne system as a function of direction and frequency?". Ferris, et al, (1966) have shown that an accurate statistical model of actual airborne antenna radiation characteristics can be generated by the use of simplified modeling techniques. It is the purpose of this report to provide additional answers to the question found above by investigating the amplitude and spectral distribution of the energy delivered to a transmitting antenna.

The problem has been divided into two parts: In the first part we will assume an input to a transmission line and calculate the amplitude of the signal delivered to the antenna as a function of the antenna and transmitter VSWR and transmission line length and loss. This is done in detail in Chapter II. The second part of the problem

1
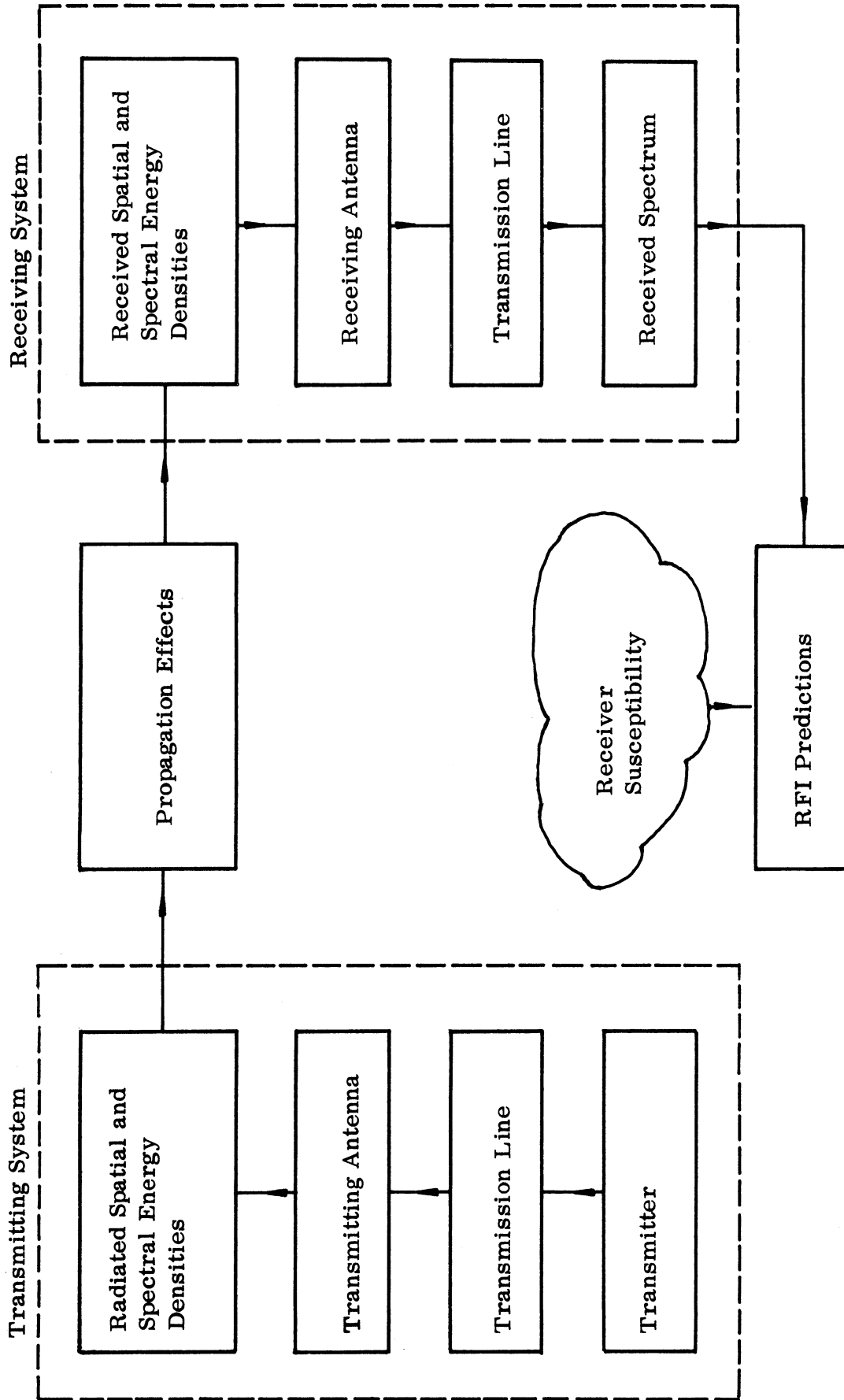
FIG. 1-1: GENERALIZED RFI PREDICTION PROBLEM

Receiving System

- Received Spatial and Spectral Energy Densities
- Receiving Antenna
- Transmission Line
- Received Spectrum

Propagation Effects

Receiver Susceptibility

RFI Predictions

Transmitting System

- Radiated Spatial and Spectral Energy Densities
- Transmitting Antenna
- Transmission Line
- Transmitter

is to determine the spectral and amplitude distribution of the energy generated in the transmitter and to measure the transmitter VSWR. Chapters III, IV and V address themselves to this portion of the problem. Techniques for measuring the transmitter VSWR have been presented in previous Michigan reports (Ferris, et al, 1966). Additional techniques are introduced in Chapter III. Chapters IV and V describe the observed transmitter behavior and various mathematical attempts at modeling the observed behavior. An adequate general model has not been discovered; however, it is not to be supposed that all feasible approaches have been tried or envisioned. Finally, Chapter VI summarizes the results and discusses the contributions to RFI predictions developed in this study.

II

POWER TRANSFER THROUGH A LOSSY TRANSMISSION LINE

The lossy line problem is not a new one and formulas are presently available in handbooks to handle this situation; however, they generally appear in a cumbersome form. It is possible to simplify the problem considerably without sacrificing accuracy or generality by dividing the problem into two parts. In part 1 we consider the power transfer for line lengths of integer multiples of half wavelengths. In part 2 the line is allowed to assume any length by approximating the entire transmission line with the appropriate number of integral half wavelengths of lossy line connected to a short section of lossless transmission line.

The characteristic impedance of a transmission line with losses is given by,

$$Z_o = \sqrt{\frac{\bar{R} + j\omega\bar{L}}{\bar{G} + j\omega\bar{C}}} \quad . \tag{2.1}$$

In Eq. (2.1),

$\bar{R}$ = series resistance of the line per unit length

$\bar{L}$ = series inductance of the line per unit length

$\bar{G}$ = shunt conductance of the line per unit length

$\bar{C}$ = shunt conductance of the line per unit length

In the consideration of the loss in transmission lines, it is convenient to assume that the characteristic impedance of the line is real. The exact condition is,

$$\frac{\bar{R}}{\bar{L}} = \frac{\bar{G}}{\bar{C}} \quad . \tag{2.2}$$

The characteristic impedance, Z_o, is then

$$Z_o = R_o + j0 \tag{2.3}$$

and

$$R_o = \sqrt{\frac{L}{C}} \quad .$$

(2.4)

For most radio frequency lines the reactive component of the characteristic impedance will be very small so that Eq. (2.2) is sufficiently satisfied for acceptable accuracy in the computation of power transfer.

2.1 Power Transfer for Line Lengths of Integer Multiples of Half Wavelengths

An equivalent circuit for the general power transfer problem is shown in Fig. 2-1. The source is modeled as an equivalent voltage source in series with an equivalent impedance at the frequency of interest. It is important to note that the source parameters, E_g and R_g, are assumed constant and independent of the terminating impedance at the source terminals.

Note also that the generator impedance and the load impedance have been chosen as real. No generality has been sacrificed because an antenna (or generator) can be connected to an appropriate short length of lossless transmission line to transform any complex impedance to a pure resistance. In this discussion the transforming line will be assumed to be of such a length that $R_a > R_o$, $R_g > R_o$. In this case, let

$$\frac{R_a}{R_o} = r_a$$

(2.5)

$$\frac{R_g}{R_o} = r_g$$

(2.6)

in which r_a and r_g are the standing wave ratios for the antenna and generator impedances.

R_g I_1

E_g E_1

Transmission Line

$Z_o = R_o$

I_a

R_a
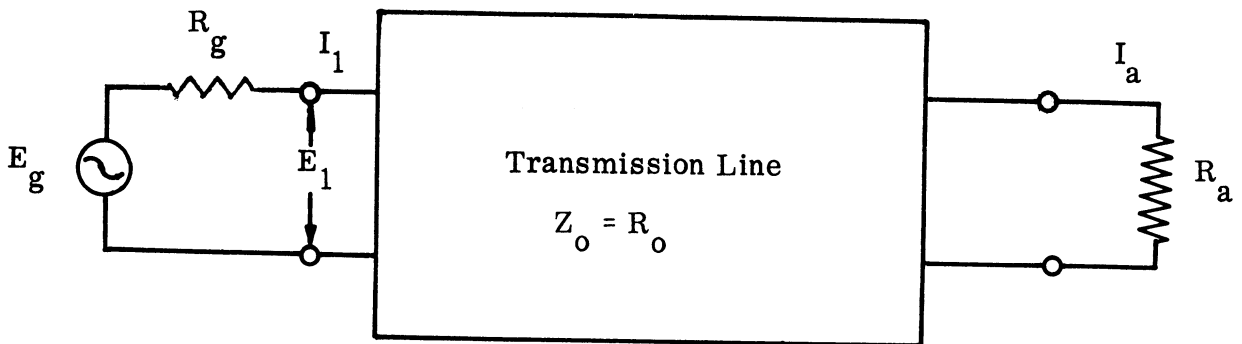
FIG. 2-1: EQUIVALENT CIRCUIT OF THE POWER TRANSFER PROBLEM

R_a = resistance of the termination of the transmission line

R_o = characteristic impedance of the transmission line

R_g = internal resistance of the equivalent generator

E_g = internal voltage of the equivalent generator

I_a = current into the load resistance

I_1 = current into the transmission line

E_1 = voltage applied to the transmission line

(All currents and voltages are rms values unless otherwise noted.)

Consider first the power transfer characteristic of the transmission line alone.
From the transmission line equations

$$I(x) = I_a \left[\cosh(\gamma x) + \frac{Z_a}{Z_o} \sinh(\gamma x) \right] \tag{2.7}$$

$$Z(x) = Z_o \left[\frac{Z_a \cosh(\gamma x) + Z_o \sinh(\gamma x)}{Z_o \cosh(\gamma x) + Z_a \sinh(\gamma x)} \right] . \tag{2.8}$$

In Eqs. (2.7) and (2.8), γ = propagation constant for the transmission line. These equations represent our circuit in Fig. 2-2 for any line length x. If we restrict the values of x that we use to exact multiples of a half wavelength, then

$$\gamma x = \alpha x + j\beta x$$

$$= \alpha x + j\beta n\pi \tag{2.9}$$

and the hyperbolic functions are:

$$\cosh(\alpha x + j\beta n\pi) = \cosh \alpha x \tag{2.10}$$

$$\sinh(\alpha x + j\beta n\pi) = \sinh \alpha x \tag{2.11}$$

Under this condition Eq. (2.7) and (2.8) contain no complex quantities.
The power into the line at $x = \ell$ is

$$P_1 = I_1^2 R_1 \tag{2.12}$$

and the power delivered to the load resistance is

$$P_a = I_a^2 R_a . \tag{2.13}$$
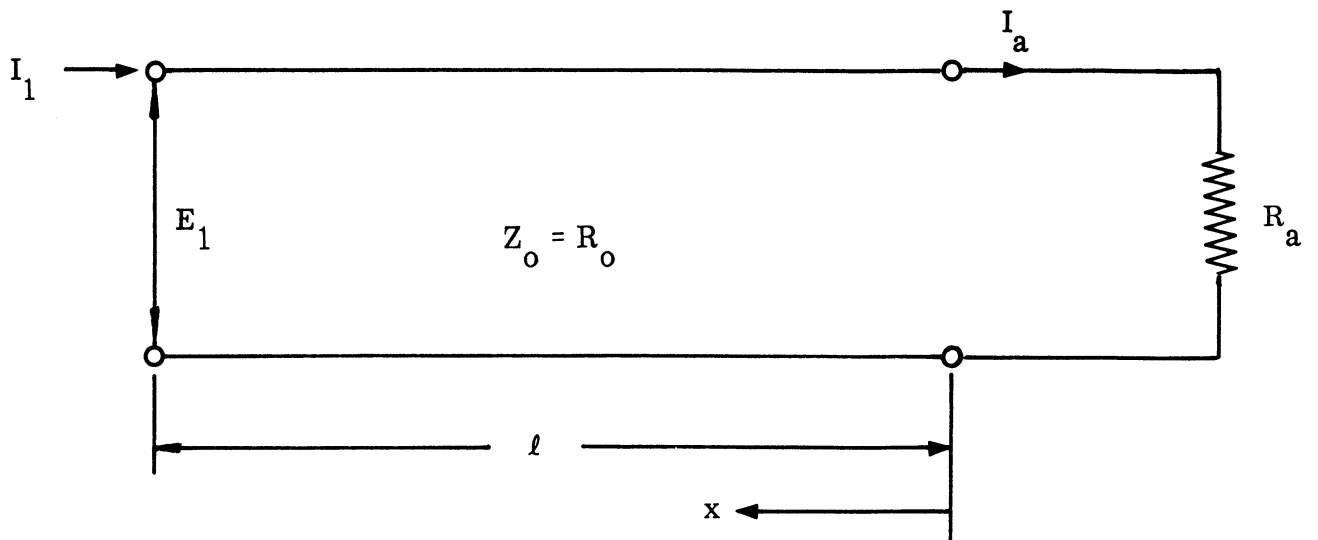
FIG. 2-2: LOSSY TRANSMISSION LINE AND LOAD

The power transfer characteristic of the transmission line is the ratio of the power delivered to the load to the power input to the line,

$$\frac{P_a}{P_1} = \frac{I_a^2 R_a}{I_1^2 R_1} \quad . \tag{2.14}$$

For this case, $Z_o = R_o$, $Z_a = R_a$, and $\ell = \dfrac{n\lambda_g}{2}$ as previously discussed so that (2.7) and (2.8) become

$$Z(x) = R_1 = R_o \frac{r_a \cosh \alpha x + \sinh \alpha x}{\cosh \alpha x + r_a \sinh \alpha x} \tag{2.15}$$

and

$$I(x) = I_1 = I_a (\cosh \alpha x + r_a \sinh \alpha x) \quad . \tag{2.16}$$

Substituting Eqs. (2.15) and (2.16) into (2.12),

$$\frac{P_a}{P_1} = \frac{r_a}{(r_a \cosh \alpha x + \sinh \alpha x)(\cosh \alpha x + r_a \sinh \alpha x)} \tag{2.17}$$

This result may be further simplified by rewriting the hyperbolic function in terms of exponentials

$$\cosh(\alpha x) = \frac{e^{\alpha x} + e^{-\alpha x}}{2} \tag{2.18}$$

$$\sinh(\alpha x) = \frac{e^{\alpha x} - e^{-\alpha x}}{2} \tag{2.19}$$

9

so that

$$\frac{P_a}{P_1} = \frac{\dfrac{4 r_a A_o}{(r_a + 1)^2}}{\left(1 - \rho_a^2 A_o^2\right)} \tag{2.20}$$

where

$$A_o = e^{-2\alpha x} \tag{2.21}$$

and ρ_a = the magnitude of the load voltage reflection coefficient = $\left(\dfrac{r_a - 1}{r_a + 1}\right)$.

Note that (2.20) includes the losses due both to line attenuation and load mismatch .

Equation (2.20), while useful, requires that P_1, the power input to the line, be known before P_a can be found. A more practical expression would be one giving P_a in terms of the generator power delivered to a matched termination, (i.e., matched to the characteristic impedance of the transmission line, R_o). Referring to Fig. 2-1 the power input to the transmission line is,

$$P_1 = \frac{E_g^2 R_1}{(R_g + R_1)^2} = \frac{E_g^2 r_1}{R_o (r_g + r_1)^2} . \tag{2.22}$$

If R_1 is replaced by a matched termination, R_o

$$P_o = \frac{E_g^2 R_o}{(R_g + R_o)^2} = \frac{E_g^2}{R_o (r_g + 1)^2} \tag{2.23}$$

and

$$\frac{P_a}{P_o} = \frac{P_a}{P_1} \cdot \frac{P_1}{P_o} . \tag{2.24}$$

10

From (2.24), in order to solve for $\dfrac{P_a}{P_o}$, is is necessary only to find $\dfrac{P_1}{P_o}$ and combine this expression with (2.20).

$$\frac{P_1}{P_o} = \frac{r_1 (r_g + 1)^2}{(r_g + r_1)^2} \qquad (2.25)$$

Substituting (2.15) into (2.25) and simplifying, one has

$$\frac{P_1}{P_o} = \frac{(r_a \cosh \alpha x + \sinh \alpha x)(\cosh \alpha x + r_a \sinh \alpha x)(r_g + 1)^2}{\left[\cosh \alpha x (r_a + r_g) + \sinh \alpha x (r_a r_g + 1)\right]^2} \qquad (2.26)$$

Rewriting in terms of exponentials as before, (2.26) becomes

$$\frac{P_1}{P_o} = \frac{(1 + A_o \rho_a)(1 - A_o \rho_a)}{\left[1 - \rho_a \rho_g A_o\right]^2} \qquad (2.27)$$

where again

$$A_o = e^{-2\alpha x}, \text{ the nominal line attenuation}$$

$$\rho_a = \text{ the magnitude of the load voltage reflection coefficient,}$$

$$\frac{r_a - 1}{r_a + 1}$$

$$\rho_g = \text{ the magnitude of the generator reflection coefficient,}$$

$$\frac{r_g - 1}{r_g + 1} \quad .$$

To find the power transferred to the load in terms of the load VSWR, generator VSWR, transmission line length, and generator power output into a matched (to the characteristic impedance of the transmission line) load, it is necessary to combine results (2.27) and (2.21) as indicated by (2.24) such that

$$\frac{P_a}{P_o} = \frac{4 r_a}{(r_a + 1)^2} \frac{A_o}{(1 - \rho_a \rho_g A_o)^2} \tag{2.28}$$

or

$$P_a = \frac{4 r_a}{(r_a + 1)^2} \frac{P_o A_o}{(1 - \rho_a \rho_g A_o)^2} . \tag{2.29}$$

Thus far the results derived have been valid only for line lengths of integer multiples of half wavelengths. However, R_1 (Eq. (2.15)) is real for line lengths which are integer multiples of quarter wavelengths. Choosing an odd multiple of a quarter wavelength, is equivalent to solving the same problem with $R_a < R_o$ or $R_g < R_o$. This causes the sign in the $(1 - \rho_a \rho_g A_o)$ factor of (2.29) to change resulting in a minimum power transfer. The result is unchanged if both $R_a < R_o$ and $R_g < R_o$.
Letting

$$F_H = 10 \log \left[1 - \rho_a \rho_g A_o\right]^{-2} \text{ (db)}$$

$$F_\ell = 10 \log \left[1 + \rho_a \rho_g A_o\right]^{-2} \text{ (db)}$$

$$A'_o = \text{nominal transmission line loss (db) (loss per foot x number of feet)} =$$
$$10 \log A_o$$

$$A_2 = 10 \log \frac{4 r_a}{(r_a + 1)^2}$$

12

(2.28) becomes

$$\frac{P_a}{P_o} = (A'_o + A_2 + F_H) \text{ (db)} \qquad \text{for} \qquad \ell = \frac{2n\lambda_g}{4} \qquad (2.30)$$

$$\frac{P_a}{P_o} = (A'_o + A_2 + F_\ell) \text{ (db)} \qquad \text{for} \qquad \ell = \frac{(2n-1)\lambda_g}{4} \qquad (2.31)$$

Figures 2-3 through 2-5 are a set of curves for the maximum and minimum power transferred as functions of r_a, r_g, and loss respectively. These results have been verified experimentally.

2.2 Power Transfer for any Length Lossy Line

The previous section derived an expression for the power transferred through a lossy line when the line length was an integer multiple of quarter wavelengths and the terminations were real. This section will generalize those results to include all other physically realizable systems, the only constraint being that the total line length be of the order of magnitude of one wavelength or greater. An equivalent circuit of the generalized problem appears in Fig. 2-6. Referring to Fig. 2-6, the total length of transmission line ℓ is divided into four lengths ℓ_1, ℓ_2, ℓ_3 and ℓ_4. Length ℓ_1 transforms Z_g to R_g; length ℓ_4 transforms Z_a to R_a; ℓ_2 is the remaining integer number of quarter wavelengths of line, and ℓ_3 is what is left over. Since the line lengths ℓ_1, ℓ_3, and ℓ_4 can be either positive or negative, the length $(\ell_1 + \ell_3 + \ell_4)$ can always be made $< \lambda_g/8$ and will be assumed lossless. Assuming $\ell_3 = 0$ for the moment,

$$\frac{P_{a1}}{P_o} = A_o + A_1 + F_H \qquad (2.32)$$

for

a) $R_a > R_o$, $R_g > R_o$, $\ell_2 = \frac{2n\lambda_g}{4}$

b) $R_a < R_o$, $R_g < R_o$, $\ell_2 = \frac{2n\lambda_g}{4}$

13

FIG. 2-3: P_a VERSUS ANTENNA AND GENERATOR VSWR.
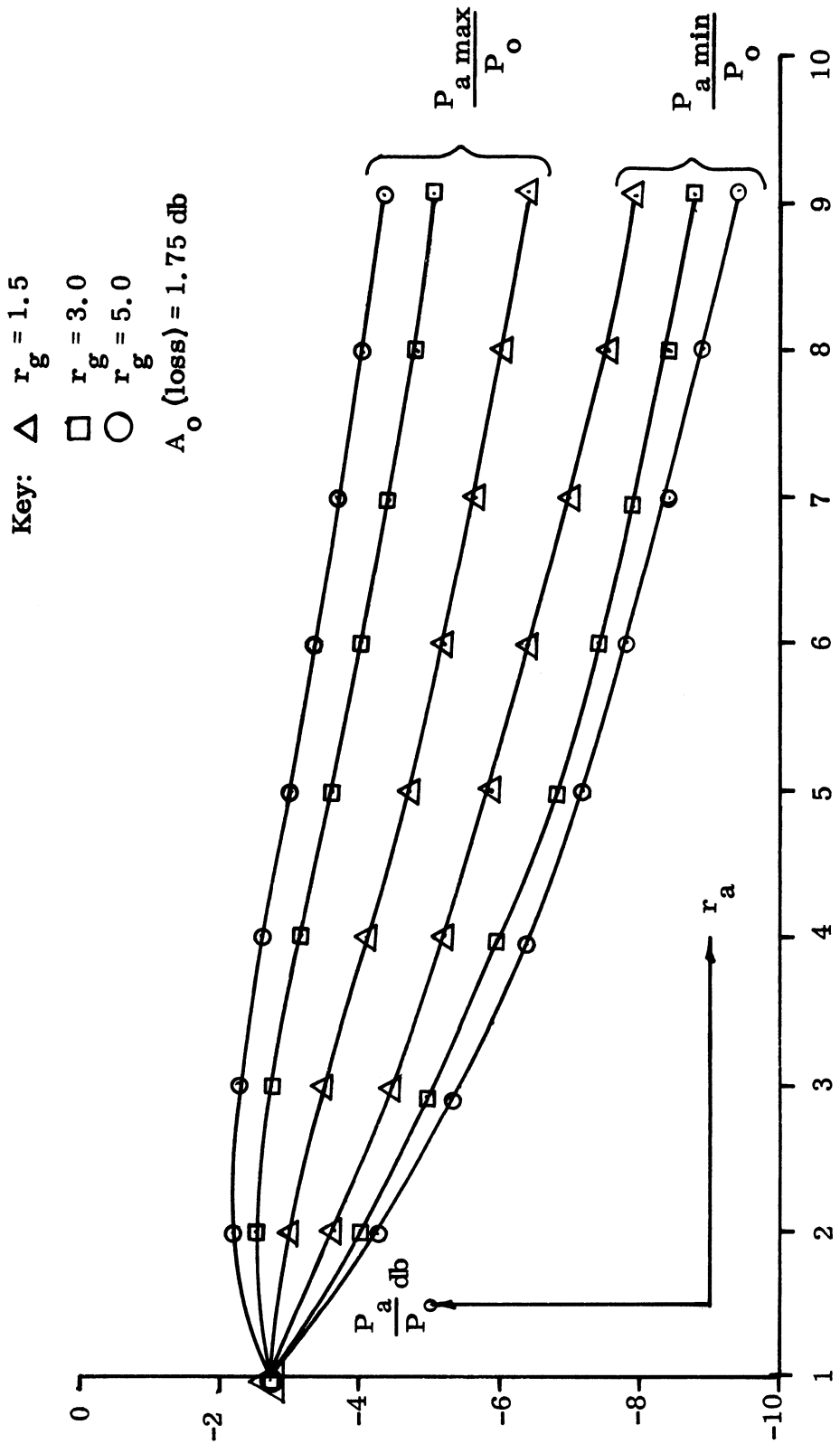
14
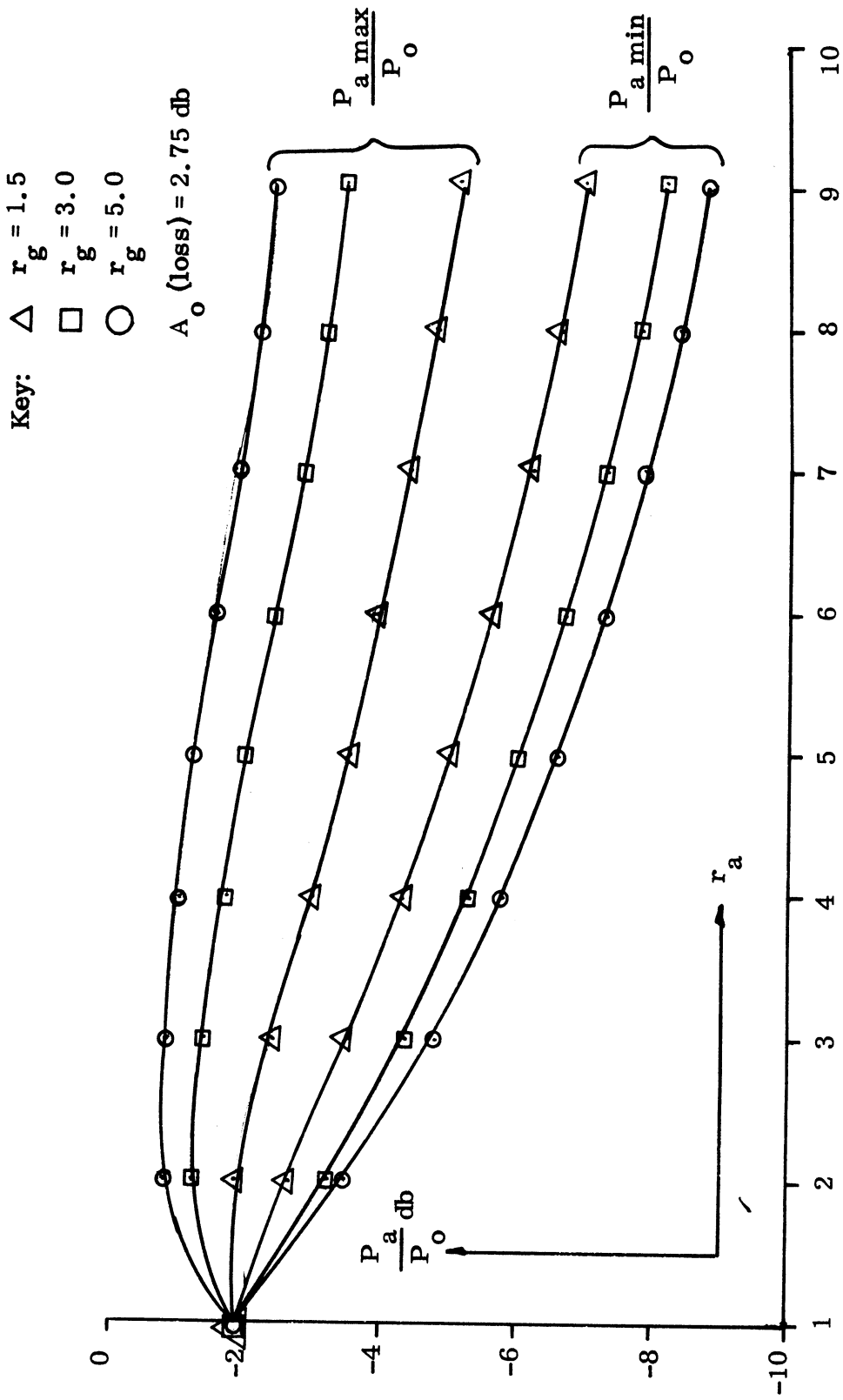
FIG. 2-4: P_a VERSUS ANTENNA AND GENERATOR VSWR.

15

FIG. 2-5: P_a VERSUS ANTENNA AND GENERATOR VSWR.

Key:

$\triangle$ $r_g = 1.5$

$\square$ $r_g = 3.0$

$\bigcirc$ $r_g = 5.0$

A_o (loss) $= 5.75$ db

$\dfrac{P_{a\ max}}{P_o}$

$\dfrac{P_{a\ min}}{P_o}$

r_a

$\dfrac{P_a}{P_o}$ db

16
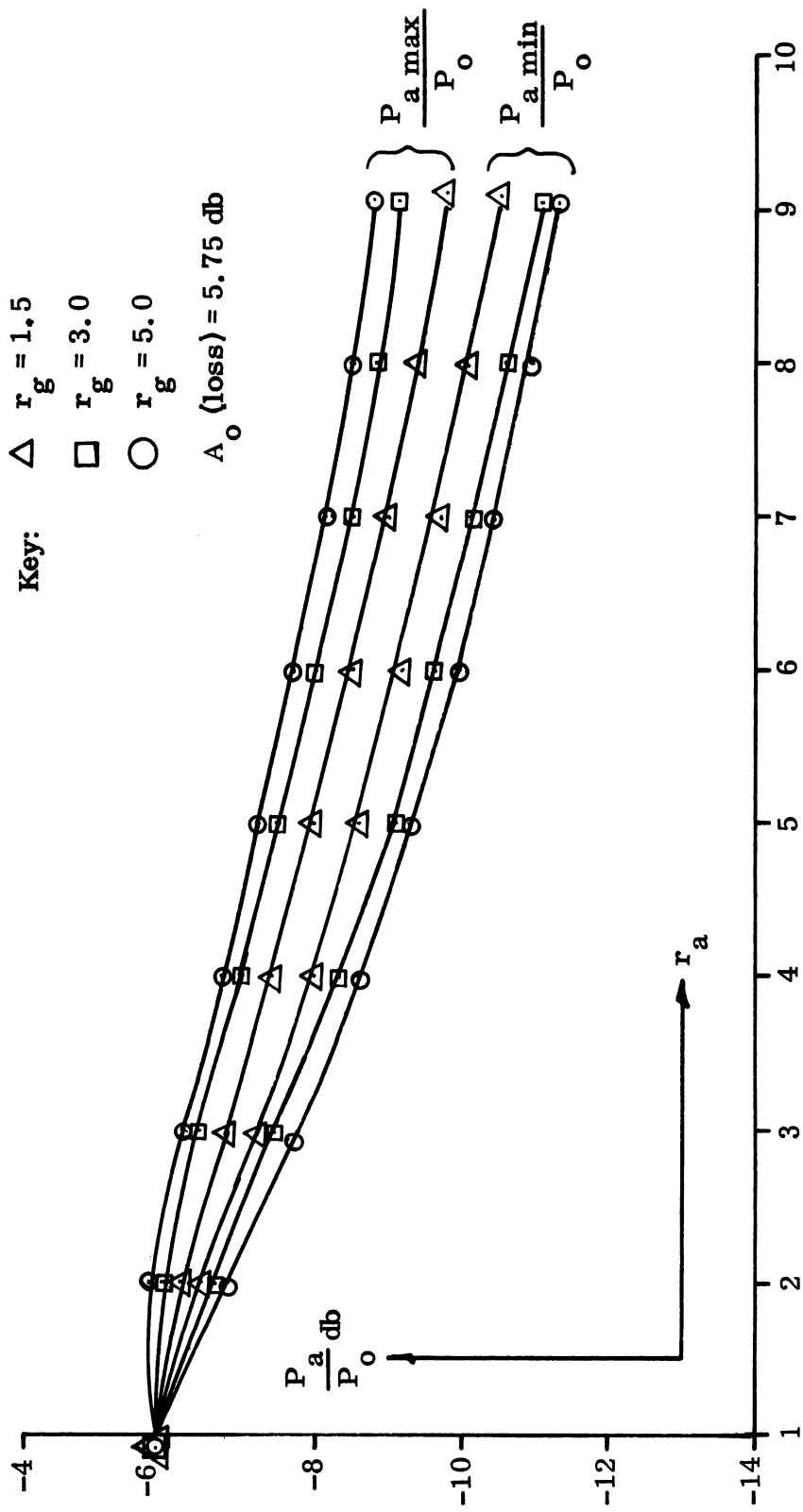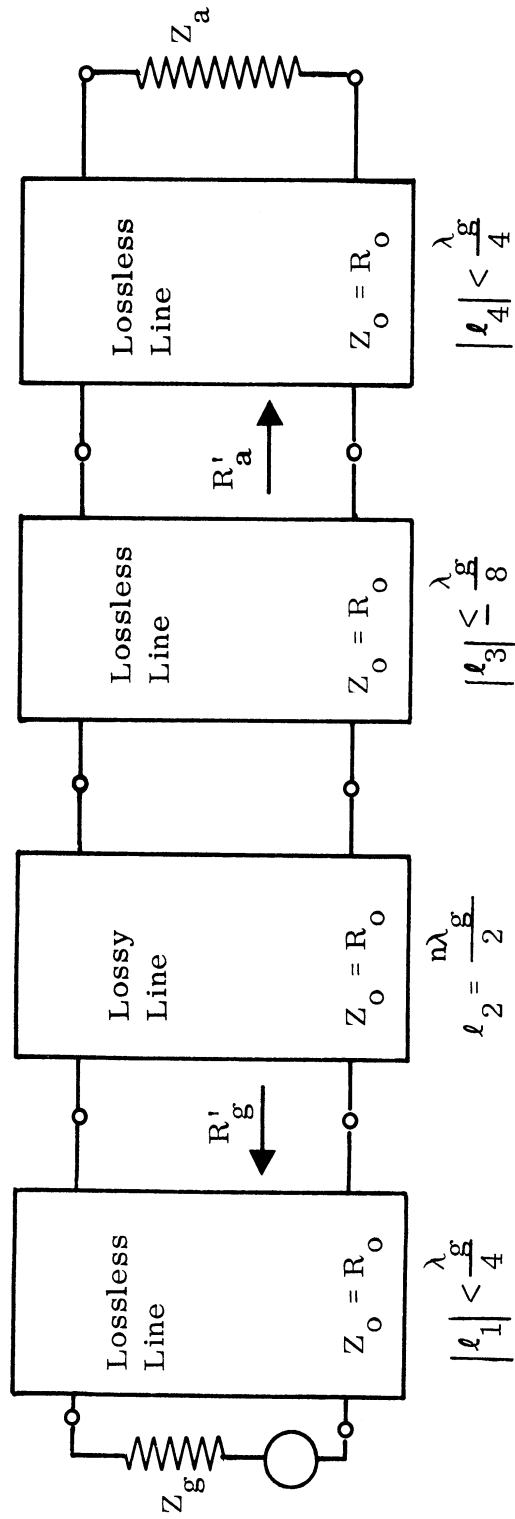
FIG. 2-6: BLOCK DIAGRAM OF THE GENERAL POWER TRANSFER PROBLEM

17

c) $R_a > R_o$, $R_g < R_o$, $\ell_2 = \dfrac{(2n-1)\lambda_g}{4}$

d) $R_a < R_o$, $R_g > R_o$, $\ell_2 = \dfrac{(2n-1)\lambda_g}{4}$

and

$$\frac{P_{a2}}{P_o} = A_o + A_1 + F_\ell \quad \text{for} \tag{2.33}$$

a) $R_a < R_o$, $R_g > R_o$, $\ell_2 = \dfrac{2n\lambda_g}{4}$

b) $R_a > R_o$, $R_g < R_o$, $\ell_2 = \dfrac{2n\lambda_g}{4}$

c) $R_a > R_o$, $R_g > R_o$, $\ell_2 = \dfrac{(2n-1)\lambda_g}{4}$

d) $R_a < R_o$, $R_g < R_o$, $\ell_2 = \dfrac{(2n-1)\lambda_g}{4}$.

The effect of length ℓ_3 will be to cause the power delivered to the load to vary between $(A'_o + A_1 + F_H)$ and $(A'_o + A_1 + F_\ell)$.

It has been shown (DeHart, 1966) that the power transfer from an idealized source through a lossless transmission line to a linear passive load can be expressed as a function of the phase angle of the load impedance.

$$P = P_{max} \frac{1}{\alpha^2 \cos^2 \phi + \sin^2 \phi} \tag{2.34}$$

where

P_{max} = the maximum power transfer for a given load

18

α^2 = the ratio of the maximum to the minimum power transfer for a given load, P_{max} / P_{min}

ϕ = the phase angle (electrical degrees) of the load .

For lossless lines, α^2 can be expressed solely in terms of the source and load VSWRs.

$$\alpha^2 = \left(\frac{r_g r_a + 1}{r_g + r_a} \right)^2 \tag{2.35}$$

where

r_g = the source VSWR

r_a = the load VSWR .

Several plots of $P(\phi)$ for various values of α^2 appear in Fig. 2-7.

For the lossy line problem, the ratio of the maximum to the minimum power available is

$$\frac{P_{a1}}{P_{a2}} = (F_H - F_\ell) \text{ (db)} . \tag{2.36}$$

This ratio becomes α^2 in (2.34), so that

$$\frac{P_a}{P_{a1}} = \frac{1}{\alpha^2 \sin^2 \beta \ell_3 + \cos^2 \beta \ell_3} \tag{2.37}$$

for those conditions given under (2.32), and

$$\frac{P_a}{P_{a2}} = \frac{1}{\alpha^2 \cos^2 \beta \ell_3 + \sin^2 \beta \ell_3} \tag{2.38}$$

for those conditions given under (2.33), where $\alpha^2 = \log^{-1} \left[\left(F_H - F_\ell \right) / 10 \right]$.
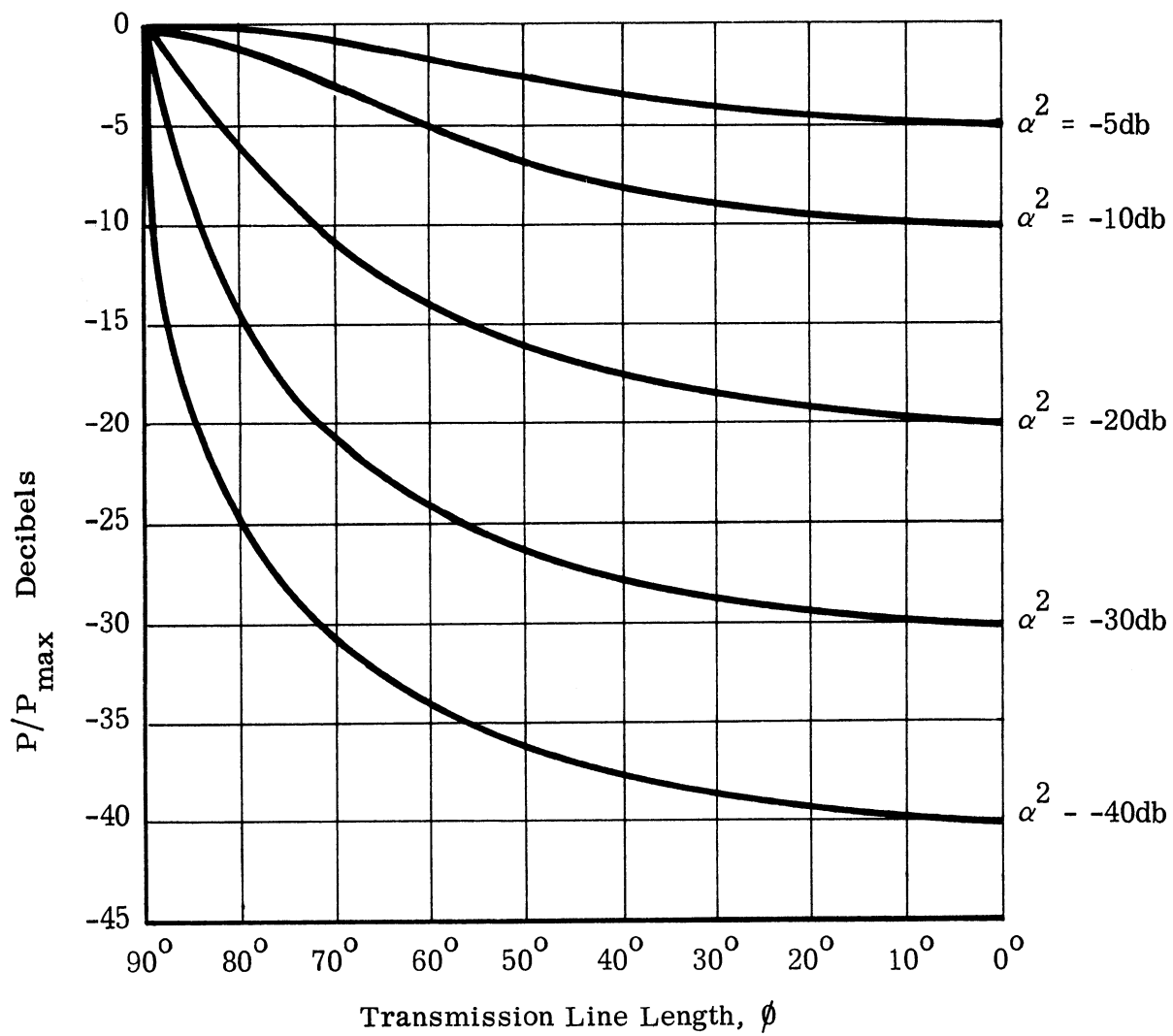
19

FIG. 2-7: POWER TRANSFER VERSUS LOSSLESS
TRANSMISSION LINE LENGTH

20

Where an exact power level is not required, it may be sufficient to solve (2.30) and (2.31) to find the maxima and minima power levels available and use (2.37) or (2.38) to determine the probability that the power level will exceed some point between those levels given by (2.30) and (2.31). To see how this can be done consider Fig. 2-8. Let P_c be some arbitrary power level between P_{a1} and P_{a2}. Associated with P_c will be some transmission line length corresponding to ϕ_c. If we assume that the transmission line length and load and generator phase angles are arbitrary, there is an equal chance that any arbitrary ϕ will occur. With this assumption the chance that ϕ will be less than ϕ_c (corresponding to a power transfer greater than P_c) is the distance from the origin to ϕ_c divided by the total abscissa.

$$\mathcal{P}(P > P_c) = \frac{\phi_c - 0^o}{90^o - 0^o} = \frac{\phi_c}{90^o} \qquad . \qquad (2.39)$$

The value of ϕ_c is given by the inverse of (2.37), so that

$$\phi_c \text{ (radians)} = \sin^{-1}\left[\left(\frac{P_{a1}}{P_c} - 1\right) \middle/ \left(\frac{P_{a1}}{P_{a2}} - 1\right)\right]^{1/2} \qquad . \qquad (2.40)$$

Thus combining (2.39) and (2.40)

$$\mathcal{P}(P > P_c) = \frac{\sin^{-1}\left[\left(\frac{P_{a1}}{P_c} - 1\right) \middle/ \left(\frac{P_{a1}}{P_{a2}} - 1\right)\right]^{1/2}}{1.5708} \qquad . \qquad (2.41)$$

2.3   Power Transfer Example

The following example illustrates how the results given above can be used to calculate the power transfer in a typical transmitter, transmission line, antenna system. Suppose we are interested in finding the power transferred from a transmitter through about $\left(\pm \ \lambda_g / 4\right)$ 33 feet of RG-9/BU to an antenna. Furthermore, let the frequency of operation be 1000 MHz, the transmitter output power be 50 watts
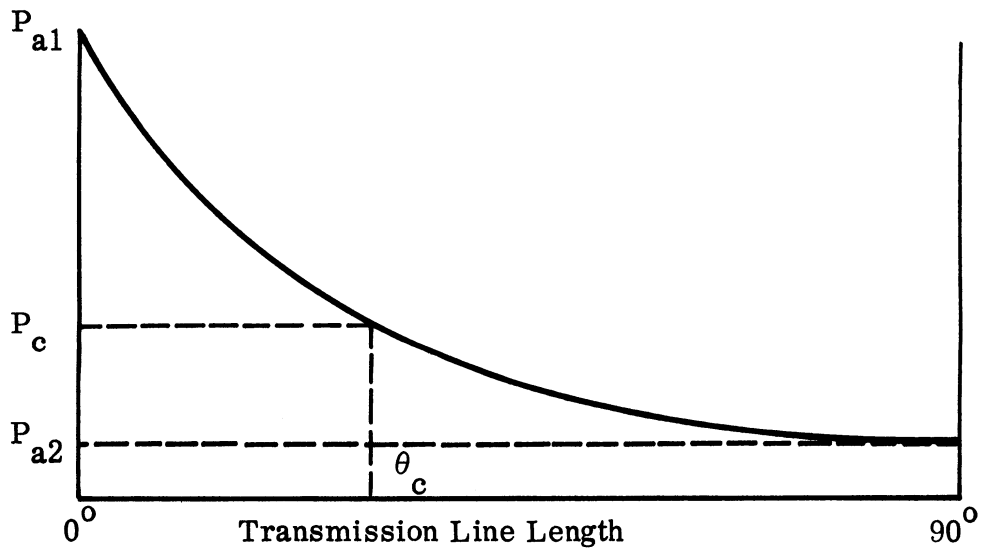
FIG. 2-8: POWER TRANSFER VERSUS TRANSMISSION LINE LENGTH

into a matched load, and the transmitter and antenna VSWR's be 2.8 and 4.2 respectively at that frequency. From a table of coaxial cable attenuation ratings the loss of RG-9/BU at 1 GHz is 9.0 db per 100 feet. Thus

$$A'_o = 9.0\,db/100' \times 33.3' = -3\,db \tag{2.42}$$

$$A_o = \log^{-1}(A'_o/10) = .501 \tag{2.43}$$

$$r_a = 4.2, \quad \rho_a = \frac{r_a - 1}{r_a + 1} = .615 \tag{2.44}$$

$$r_g = 2.8, \quad \rho_g = \frac{r_g - 1}{r_g + 1} = .474 \tag{2.45}$$

$$A_2 = 10 \log 4\,r_a/(r_a + 1)^2 = -2.07\,db \tag{2.46}$$

$$F_H = 10 \log \left[1 - \rho_a \rho_g A_o\right]^{-2} = +1.38\,db \tag{2.47}$$

$$F_\ell = 10 \log \left[1 - \rho_a \rho_g A_o\right]^{-2} = -1.18\,db \quad . \tag{2.48}$$

From (2.32) and (2.33),

$$\frac{P_{a1}}{P_o} = (A'_o + A_2 + F_H) = -3.69\,db \tag{2.49}$$

and

$$\frac{P_{a2}}{P_o} = (A'_o + A_2 + F_\ell) = -6.25\,db \quad . \tag{2.50}$$

Since $P_o = 50\,w$,

$$P_{a1} = 50 \times \log^{-1}\left(\frac{-3.69}{10}\right) = 21.3\,w \tag{2.51}$$

$$P_{a2} = 50 \times \log^{-1}\left(\frac{-6.25}{10}\right) = 11.9 \text{ w} \quad . \tag{2.52}$$

That is, the maximum power that can be delivered to the antenna specified by this transmitter at this frequency is 21.3 w and the minimum is 11.9 w. The power will vary between these limits as the transmission line length is varied over a half wavelength but will never exceed P_{a1} nor be exceeded by P_{a2} for these conditions. The probability that the power output will exceed some arbitrary value, say 15 watts, is given by (2.41). In this case

$$p\left(P_a > 15\right) = \frac{\sin^{-1}\left[\left(\frac{21.3}{15} - 1\right)\left(\frac{21.3}{11.9} - 1\right)\right]^{1/2}}{1.5708}$$

$$= \frac{\sin^{-1}(.730)}{1.5708} = .516 \tag{2.53}$$

indicating that for this system there is about a 50 per cent chance that the power delivered to the antenna will exceed 15 watts at this frequency.

2.4 Concluding Remarks

In this section we have developed equations which describe the power transfer through a lossy transmission line. Since the development approximates a lossy line with a series of lossless and lossy lines it may not be accurate for very short lines with high losses. However, such transmission lines are undesirable in most practical systems and seldom encountered. The maximum line length assumed lossless is $\lambda_g/8$, making this a very good approximation for all but the special case noted above.

One of the inputs to the power transfer expressions is the transmitter VSWR. Techniques for measuring source VSWR's have been discussed (Ferris, et al 1966) and a general method is developed in the next chapter.

Finally, the transmitter parameters were assumed to remain constant with respect to time and load variations. Chapters IV and V investigate the validity and applicability of this assumption.

III

SOURCE IMPEDANCE MEASUREMENT

Expressions describing the power transfer from a source, through a lossy transmission line, to an antenna were developed in the previous chapter. All of the system parameters necessary to evaluate these expressions are readily available from standard measurements except, perhaps, the source VSWR. Two methods for measuring source VSWR and impedance have been described (Ferris, et al 1966). Both methods rely on shifting the phase of the source termination by at least 90 electrical degrees. This technique, while adequate for laboratory measurements on transmitters whose parameters do not vary as a function of the load impedance, is unsatisfactory for a wide range of sources. The basis for a scheme which minimizes the change of load impedance necessary for transmitter impedance measurements is described below.

One concept for measuring the transmitter impedance is shown schematically in Fig. 3-1. The transmitter is modeled by an equivalent current source $I_t = I_t \sin \omega t$, and internal admittance Y_t, the load is Y_ℓ. The voltage E is measured for two values of Y_ℓ, Y_1 and Y_2. The following equations apply.

$$I_t = E_1 (Y_t + Y_1) \tag{3.1}$$

$$I_t = E_2 (Y_t + Y_2) \quad . \tag{3.2}$$

Combining equations (3.1) and (3.2),

$$E_1 (Y_t + Y_1) = E_2 (Y_t + Y_2) \quad . \tag{3.3}$$

From which,

$$Y_t = \frac{E_1 Y_1 - E_2 Y_2}{E_2 - E_1} = \frac{Y_1 - \dfrac{E_2}{E_1} Y_2}{\dfrac{E_2}{E_1} - 1} \quad . \tag{3.4a, b}$$
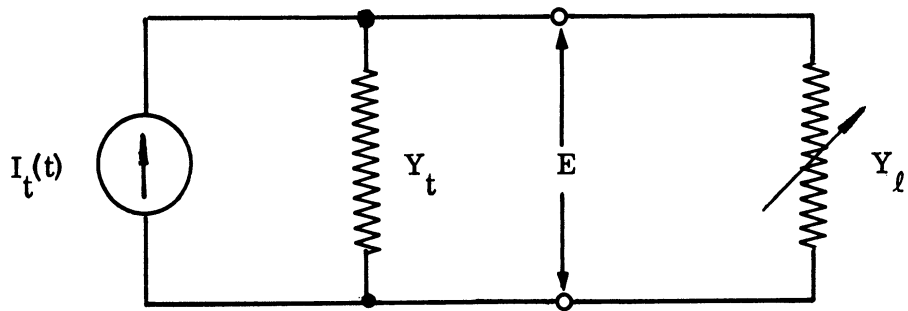
25

FIG. 3-1: TRANSMITTER EQUIVALENT CIRCUIT
AND VARIABLE LOAD

It must be remembered that Y_t, Y_1, Y_2, E_1, and E_2 are in general complex quantities, hence

$$Y_t = G_t + j B_t \qquad (3.5a)$$

$$Y_1 = G_1 + j B_1 \qquad (3.5b)$$

$$Y_2 = G_2 + j B_2 \qquad (3.5c)$$

$$E_1 = \left| E_1 \right| e^{j\theta_1} \qquad (3.5d)$$

$$E_2 = \left| E_2 \right| e^{j\theta_2} \qquad . \qquad (3.5e)$$

The ratio E_2/E_1 becomes,

$$\frac{E_2}{E_1} = \left| \frac{E_2}{E_1} \right| \frac{e^{j\theta_2}}{e^{j\theta_1}} = \left| \frac{E_2}{E_1} \right| e^{j(\theta_2 - \theta_1)} \qquad (3.6a)$$

$$= \left| \frac{E_2}{E_1} \right| \left[\cos (\theta_2 - \theta_1) + j \sin (\theta_2 - \theta_1) \right] \qquad . \qquad (3.6b)$$

Substituting equations (3.5a, b, c) and (3.6b) into (3.4) and setting

$$\left| \frac{E_2}{E_1} \right| \cos (\theta_2 - \theta_1) = a \; ; \qquad \left| \frac{E_2}{E_1} \right| \sin (\theta_2 - \theta_1) = b$$

for convenience,

$$G_t + j B_t = \frac{G_1 + j B_1 - (a + jb)(G_2 + j B_2)}{(a + jb) - 1} \qquad . \qquad (3.7)$$

Separating the real and imaginary components of (3.7),

$$G_t = \frac{G_1 (a - 1) + B_1 (b) + G_2 (-a^2 + a - b^2) + B_2 (-b)}{(a - 1)^2 + b^2} \qquad (3.8a)$$

$$B_t = \frac{G_1 (-b) + B_1 (a - 1) + G_2 (b) + B_2 (-a^2 + a - b^2)}{(a - 1)^2 + b^2} \, . \qquad (3.8b)$$

Eqs. (3.8a, b) and Fig. 3-1 describe a very general method for determining a transmitter's output admittance. One specific variation of Fig. 3-1 is shown in Fig. 3-2. It is interesting to note parenthetically that the methods previously described for determining the transmitter impedance are simply special cases of (3.8a, b) where $(\theta_2 - \theta_1) = \pi/2$ and Z_1 is transformed to the point where $Z'_t = R'_t$ implying that $Y'_t = G'_t$.

In Fig. 3-2, Y_s is a small admittance which can be switched into the circuit. Thus Y_1 and Y_2 (Eqs. (3.4a, b)) would become Y_1 and $Y_1 + Y_s$ respectively. In practice, when dealing with a transmitter whose output parameters vary with load admittance, one could choose Y_1 equal to the actual load admittance which would be placed on the transmitter terminals in actual service. Y_s could then be chosen sufficiently small (commensurate with measurement equipment accuracy) to effectively preclude variations of the transmitter parameters.
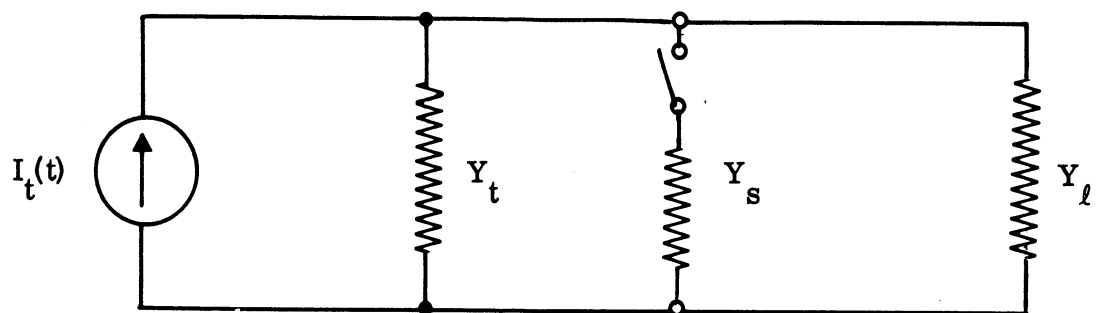
FIG. 3-2: A VARIABLE LOAD METHOD FOR TRANSMITTER
IMPEDANCE MEASUREMENT

IV

EXPERIMENTAL TRANSMITTER OUTPUT CHARACTERISTICS

In the last two chapters we developed the equations necessary to determine the power delivered from a source to an antenna for those sources whose parameters do not vary as a function of the terminating impedance. This chapter will show to what extent two typical military transmitters, an RT-178/ARC-27 and ARC-34, satisfy these requirements and discuss how the model can be modified to accomodate sources whose behavior deviates from the model.

The first observation we make of the transmitters is that, unlike the model in the previous sections, the output is polychromatic. Thus the source model of Fig. 2-1 is expanded to that of Fig. 4-1. This model consists of n independent sources, one at each of the n frequencies of interest. Note that this does not modify any of the results previously given. It merely adds the requirement that the measurements and calculations be performed at each frequency at which an output exists. It remains to determine under what conditions Fig. 4-1 mirrors the transmitter's behavior.

The major analytical tool used in this study for evaluating the transmitters' behavior is contours of constant power output at each frequency of interest plotted as a function of the terminating impedance on a Smith Chart. Such diagrams are commonly known as Rieke diagrams. Expressions of constant power contours for the model in Fig. 2-1 are developed in Appendix A.

4.1   Output Behavior at the Fundamental

Using the equipment setup diagrammed in Fig. 4-2, the diagrams in Fig. 4-3 were obtained for an ARC-27 at a fundamental frequency of 300 MHz. Notice that the fundamental output is very similar to the results predicted by the model for load VSWR's up to and exceeding 4:1. Similar results were witnessed when the transmitter was tuned for other fundamental output frequencies.
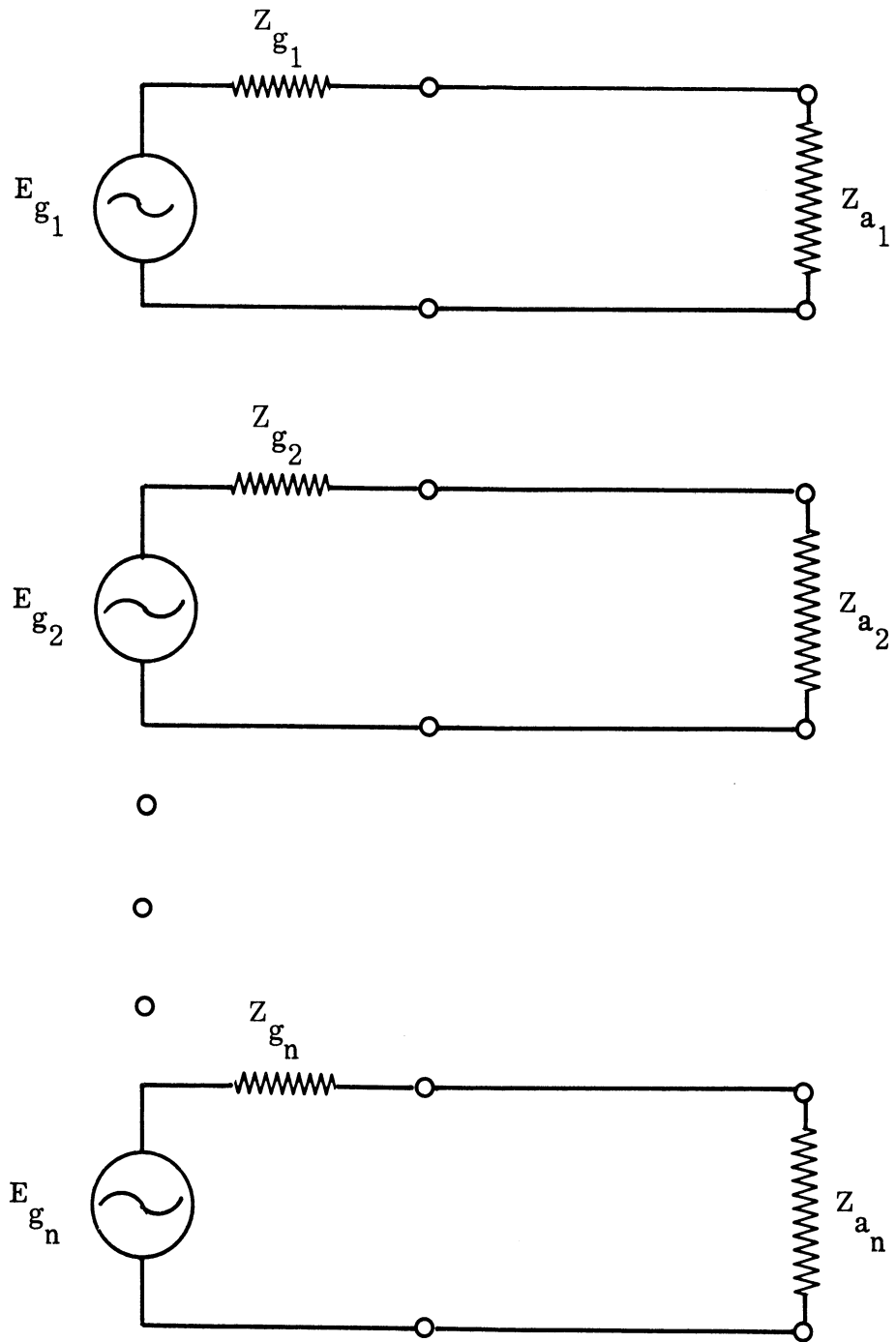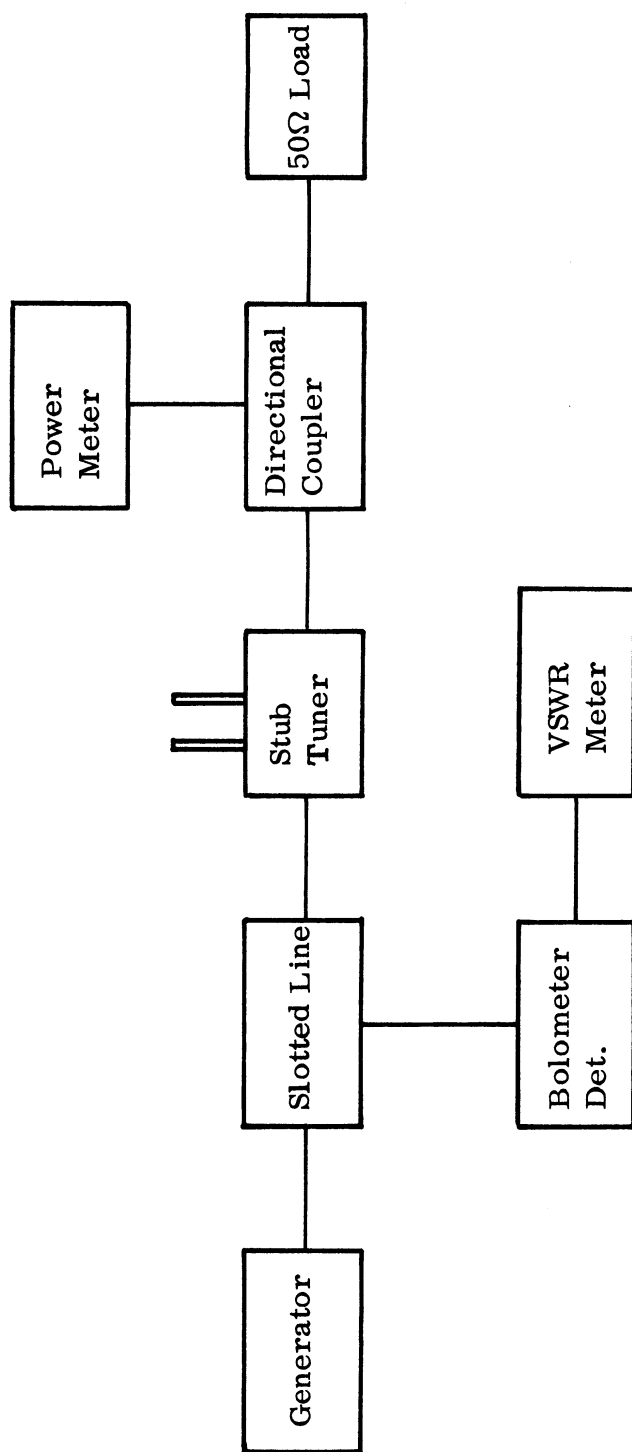
FIG. 4-1: MULTIPLE HARMONIC GENERATOR MODEL

FIG. 4-2: EQUIPMENT BLOCK DIAGRAM FOR
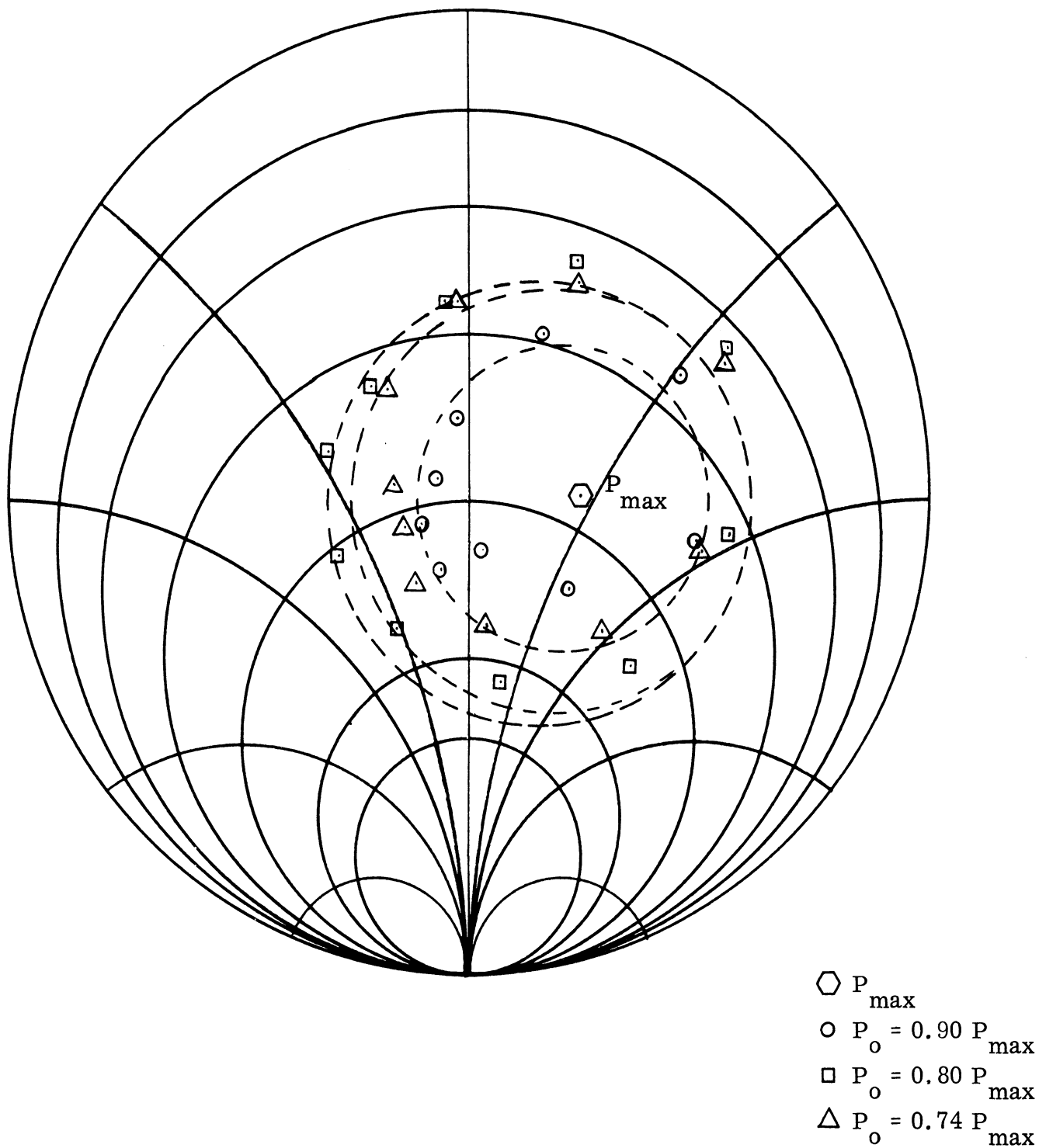EXPERIMENTAL RIEKE DIAGRAMS

FIG. 4-3: RIEKE DIAGRAM OF THE FUNDAMENTAL OUTPUT OF AN ARC-27.

4.2 Output Behavior at the Harmonics

An identical set of measurements was taken at the second and third harmonic frequencies by replacing the bolometer and power meter in Fig. 4-2 with frequency selective detectors. The results indicated that the second and third harmonics did not follow the behavior predicted by the model. A new series of experiments was devised to determine the cause of the deviations from the model behavior.

4.2.1 Inter-harmonic Coupling

The first experiment is engineered to see what influence the termination at the second harmonic has on the transmitter output at the third harmonic when the fundamental is terminated in the reflectionless load.

The military type RT-178/ARC-27 transmitter was connected into the measurement setup shown in Fig. 4-4, and the second harmonic power delivered to a matched (50 Ω) load was measured as a function of the third harmonic load. Inspection of the data in Fig. 4-5 reveals a total second harmonic relative power variation of $\pm$ 1.7 db for third harmonic load VSWR's ranging from 2.0:1 to 8.4:1. Measurements of the power at the third harmonic as a function of the load at the second harmonic were also performed utilizing the equipment arrangement of Fig. 4-4. The data is presented in Fig. 4-6. Note that there was a maximum power variation of $\pm$ 1.1 db at the third harmonic for a 10:1 VSWR at the second harmonic when the third harmonic component was terminated in a matched load.

The impedance measurements were performed with a slotted line, receiver, bolometer detector, and a standard VSWR amplifier at both harmonics. The loads and power measurement equipment were very similar for both measurements. Referring to Fig. 4-4, the 700 MHz low pass filter and a 50 Ω termination provided a matched load at the second harmonic and a high reactance at the third harmonic. The real part of the third harmonic load impedance was varied with a 50 Ω variable attenuator, while a line stretcher provided continuously variable phase. In Fig. 4-4, a large reactance at the second harmonic was provided by a single shorted stub adjusted at the second harmonic to $\lambda/2$. When so adjusted, the stub was $\lambda/4$ at
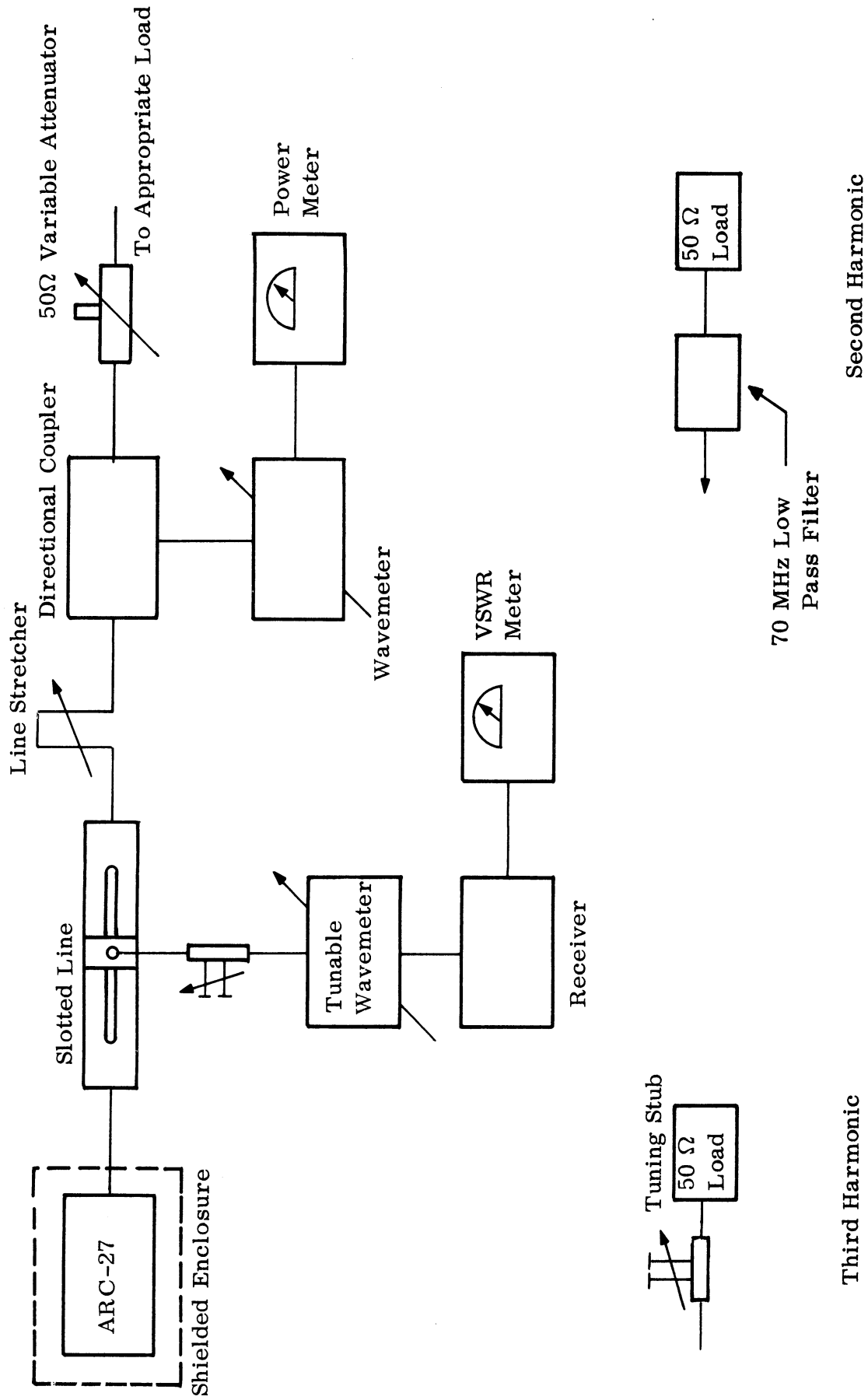
FIG. 4-4: EXPERIMENTAL POWER TRANSFER CONTOUR EQUIPMENT ARRANGEMENT
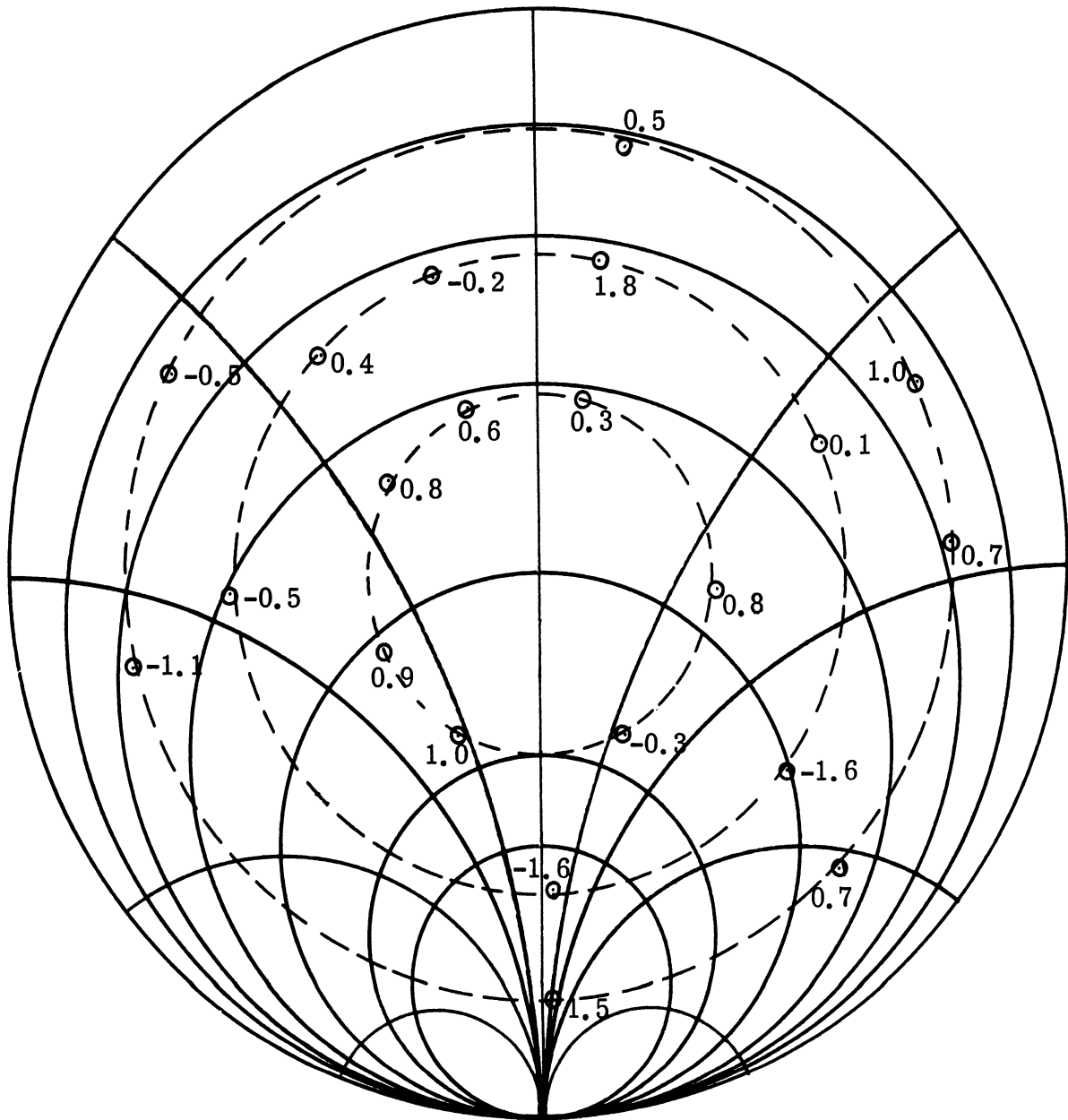
35

FIG. 4-5: RELATIVE POWER OUTPUT (db) AT THE SECOND HARMONIC
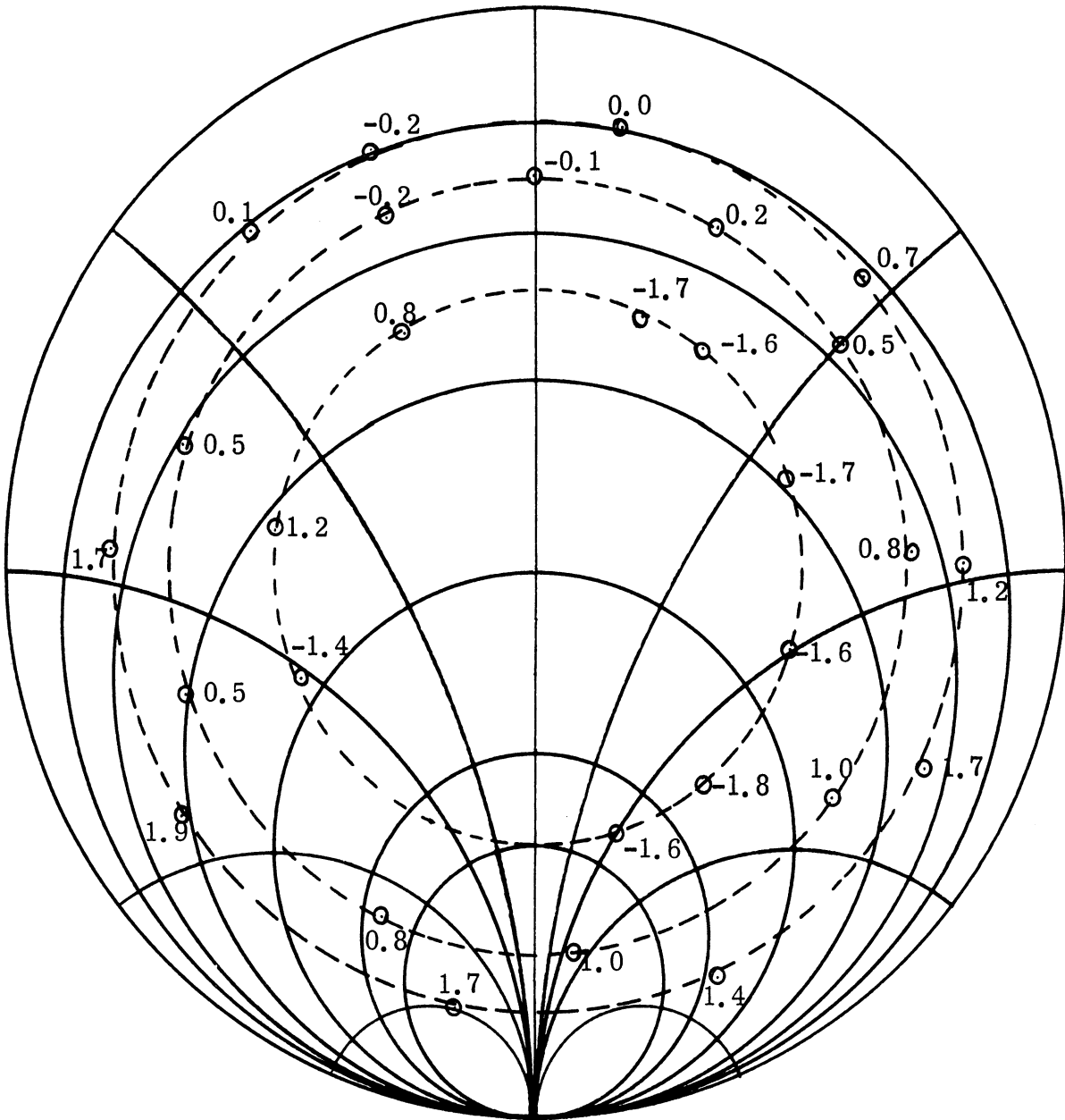FREQUENCY VERSUS IMPEDANCE AT THE THIRD HARMONIC

FIG. 4-6: RELATIVE POWER OUTPUT (db) AT THE THIRD HARMONIC
FREQUENCY VERSUS IMPEDANCE AT THE SECOND HARMONIC

the fundamental and $3/4\lambda$ at the third harmonic, allowing these frequencies to be terminated by the matched $50\,\Omega$ load. The impedance at the second harmonic was varied with a line stretcher and variable attenuator as described above. The power measurement equipment consisted simply of a directional coupler, band pass wavemeter, and power meter. The power sampled at the incident port was proportional to the power absorbed by the load since the load was matched at the frequency of interest.

The power output variations at one harmonic due to load impedance variations at the others are relatively small when the fundamental and harmonic of interest are matched with a reflectionless termination. At this point two questions come naturally to mind:

1) How is the power output at a given harmonic affected by the termination at that frequency, and

2) How is the output at the harmonic influenced by the match at the fundamental?

4.2.2 Isolated Harmonic Behavior

To answer the first question, an experiment was run in which the power output at the second harmonic was plotted as a function of the terminating impedance at that frequency while the fundamental and third harmonic were kept matched. The experiment was then repeated at the third harmonic. The equipment arrangement was identical to that diagrammed in Fig. 4-4 except that the loads were interchanged. The results are presented in Figs. 4-7 and 4-8. This time the power output appears plotted as a function of load phase angles at constant values of VSWR. The smooth curves are the results predicted by the model and Eq. (2.34). The reason for the change of data format is simply that it is more convenient to measure power output versus load impedance than vice versa. Notice that the experimental results are within about ± 1 db of the power levels predicted by the model. Thus we conclude that the model is an adequate representation of the transmitter behavior so long as the fundamental is matched with a reflectionless termination.
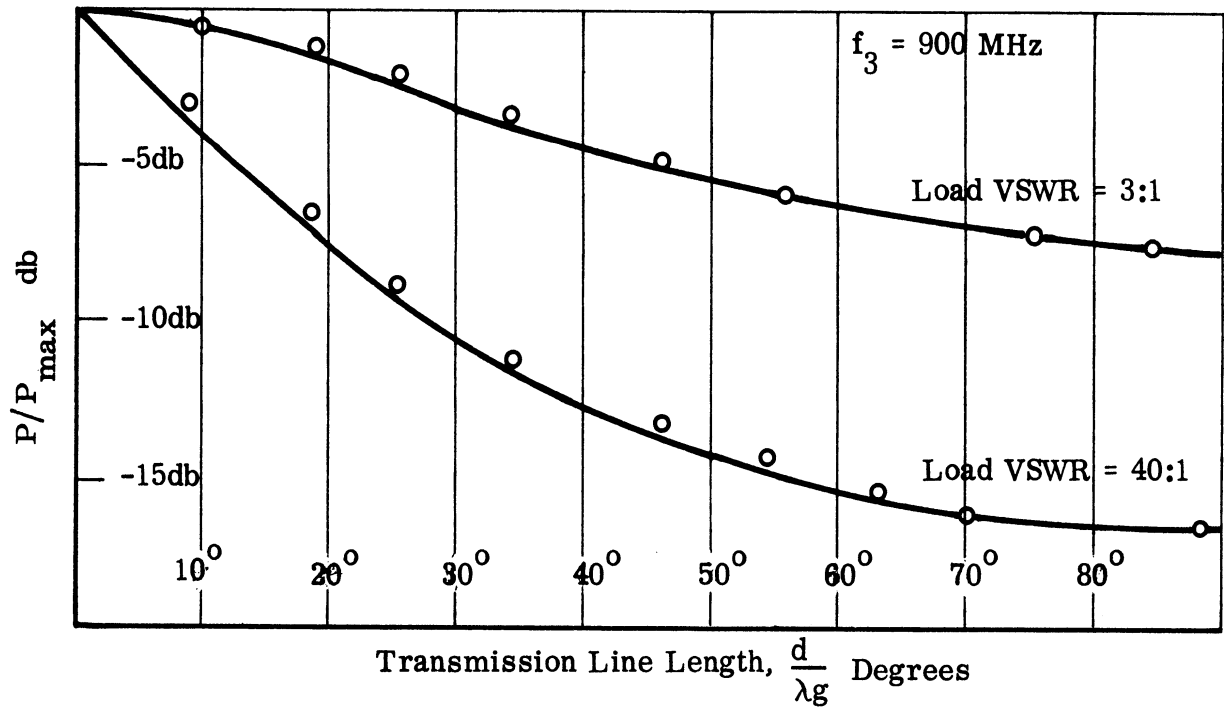
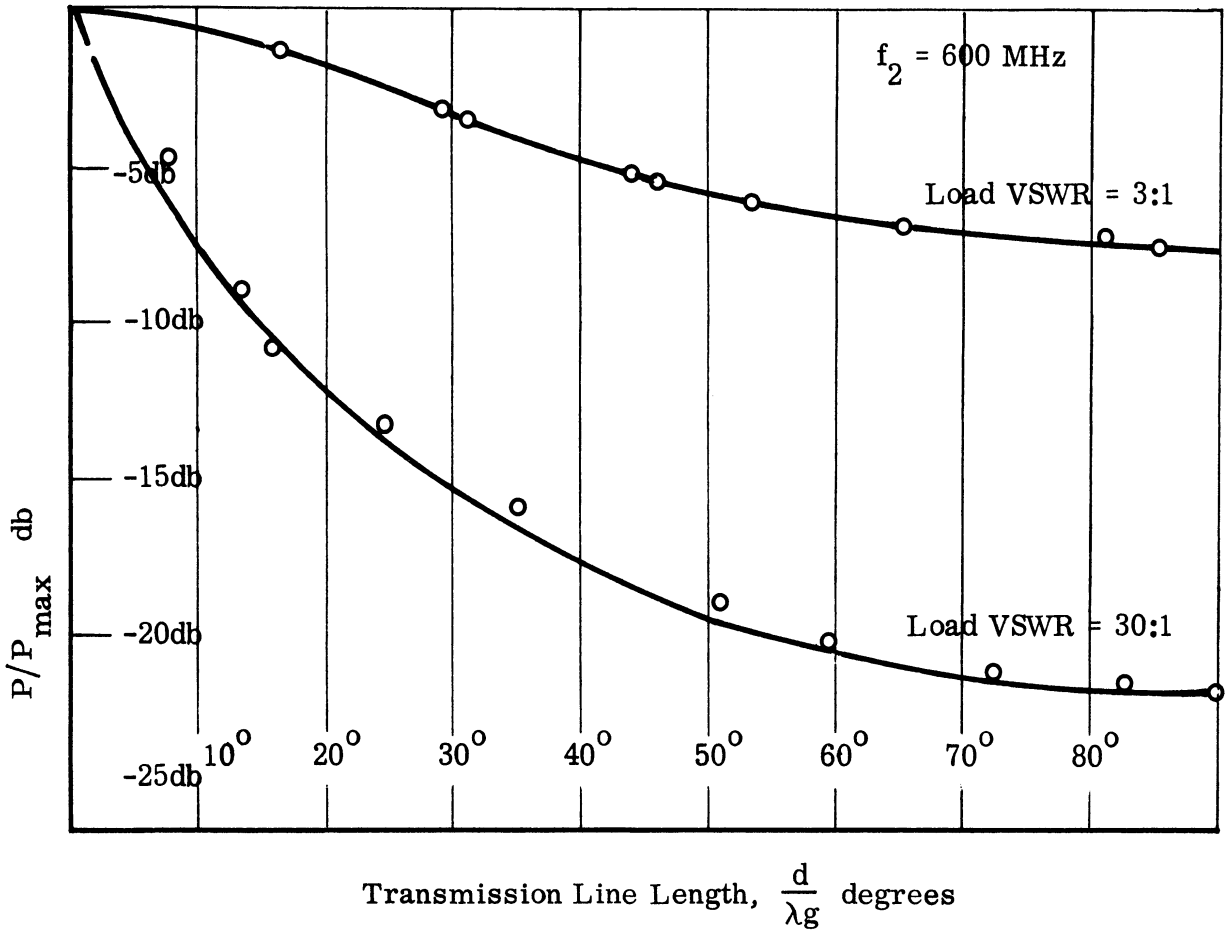FIG. 4-7: POWER TRANSFER VERSUS TRANSMISSION LINE LENGTH

FIG. 4-8: POWER TRANSFER VERSUS TRANSMISSION LINE LENGTH

4.2.3 Harmonic Rieke Diagrams

We will now investigate the influence of the terminating impedance at the fundamental frequency on the power output at harmonic frequencies when the harmonics are terminated in a matched load. The test equipment arrangement is diagrammed in Fig. 4-9. The stub tuner is adjusted to provide a match at the harmonic of interest. The attenuator and variable length line provide a continuously variable magnitude and phase of the terminating impedance at the fundamental frequency. The results are plotted as contours of constant power output at the harmonic of interest versus the impedance at the fundamental; ergo the term "Harmonic Rieke Diagram".

Figures 4-10 through 4-20 are harmonic Rieke diagrams of three different transmitters at their second and third harmonic response. Included on the diagrams are the fundamental and harmonic frequencies of operation, the transmitter type and serial number, and the total variation of harmonic output power as the load at the fundamental varies around a constant 3:1 VSWR mismatch. Figures 4-10, 4-11, and 4-12 are all of ARC-27's operating at the same frequency. After the data representing 4-11 was collected the transmitter malfunctioned and had to be repaired and realigned. The same set of measurements was repeated at the same frequency. The results appear in Fig. 4-12. It is noteworthy that when properly adjusted the power variations for both ARC-27's at the second harmonic frequencies measured were about $\pm$ 1.5 db. The model diagrammed in Fig. 4-1 would be adequate for this type of behavior. Unhappily, the power variations of the ARC-27 at the third harmonic (Figs. 4-15 through 4-17) range from $\pm$ 6 db to $\pm$ 9 db around a circle of constant 3:1 VSWR at the fundamental. There seems to be some similarity between the ARC-27 third harmonic diagrams. The maximum power output corresponds to a fundamental terminating impedance in the first quadrant in all three case, but there is also a peaking early in the third quadrant at 900 MHz. The ARC-34 displays considerably more variation at the second harmonics. Typical ranges are $\pm$ 4 to 5 db for constant 3:1 VSWR's at the fundamental. Third harmonic variations of the ARC-34 are even more extreme.

41
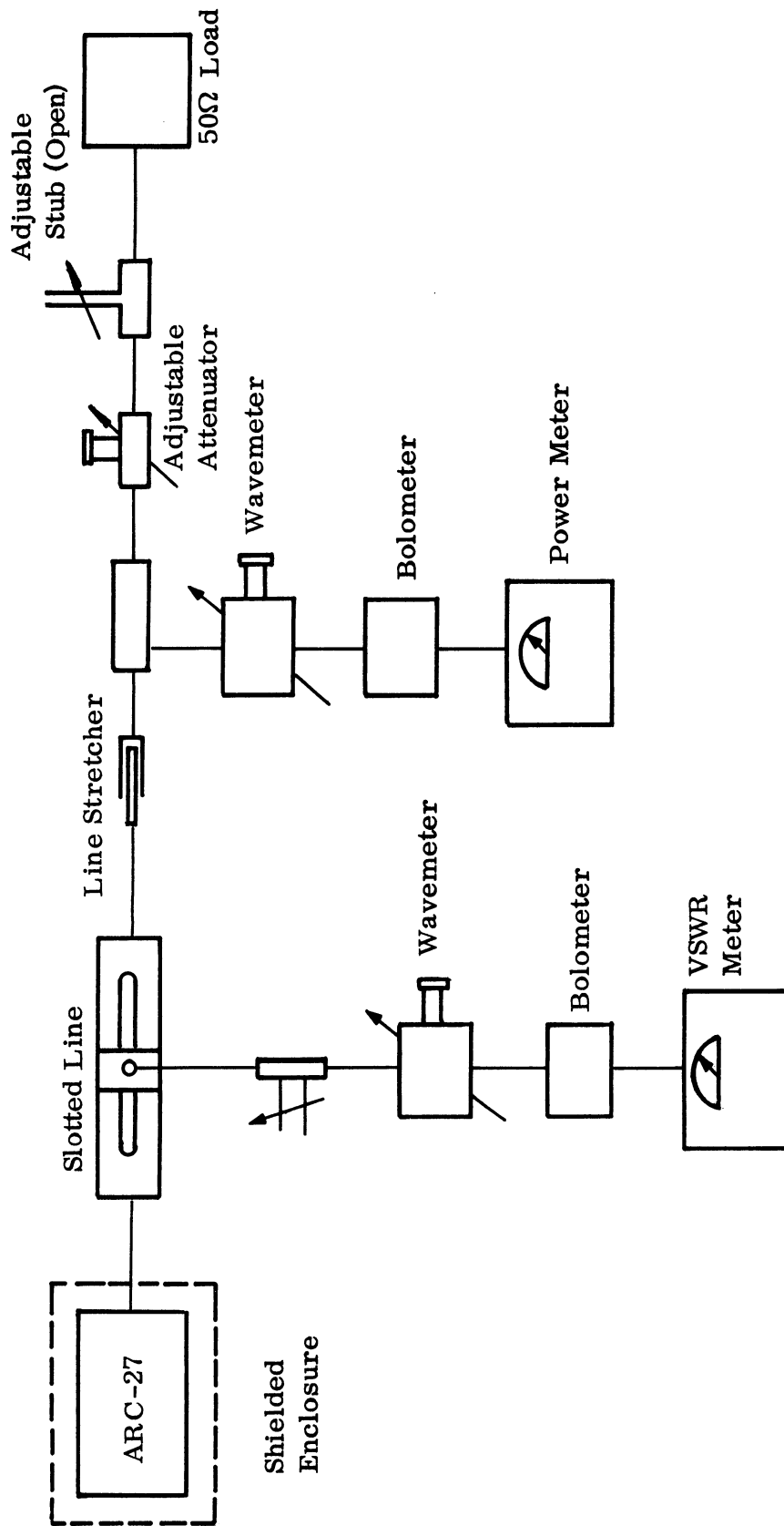
FIG. 4-9: EXPERIMENTAL "HARMONIC RIEKE DIAGRAM" EQUIPMENT ARRANGEMENT
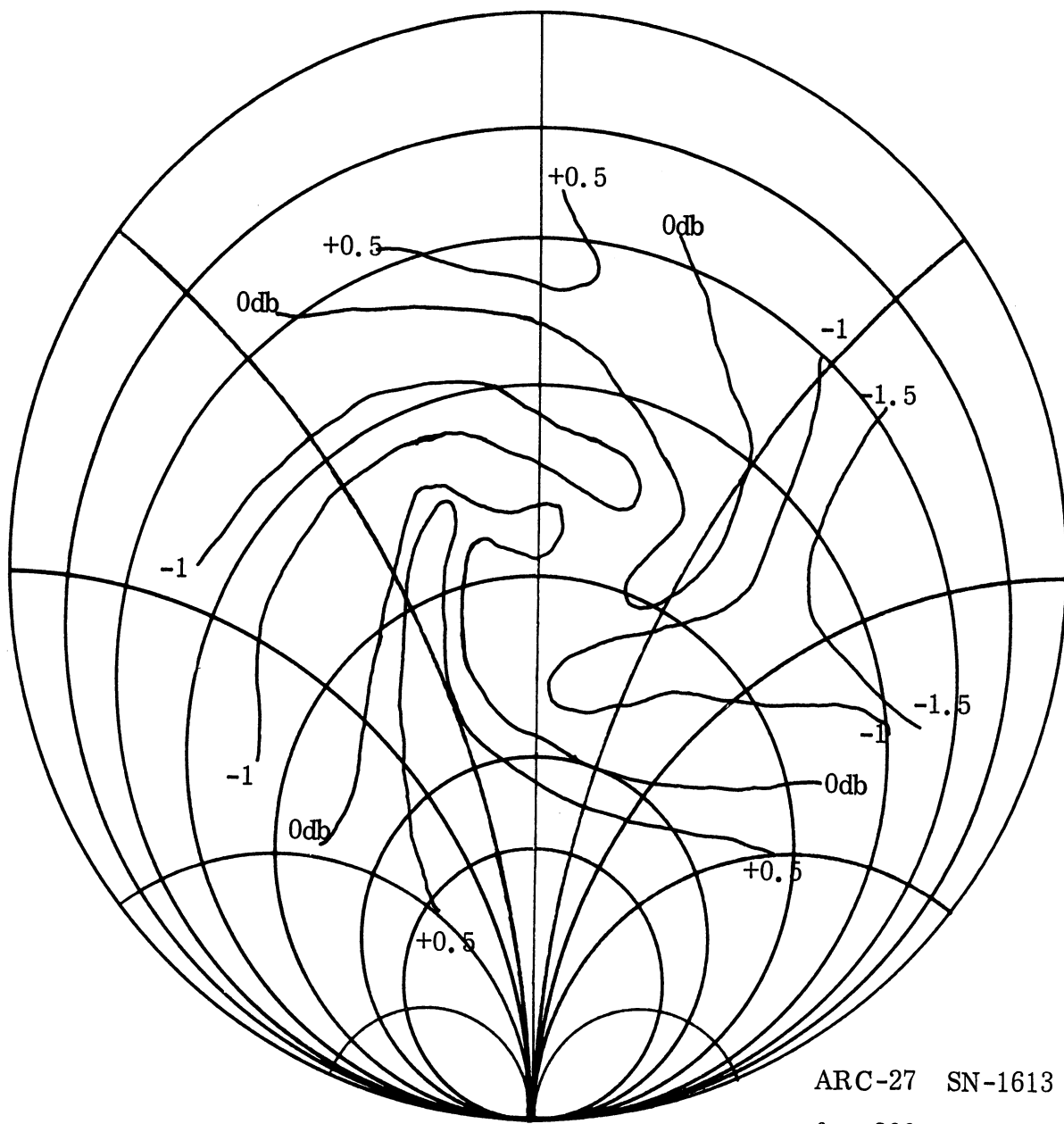
ARC-27   SN-1613

f_o = 300 MHz

f_n = 600 MHz

Total Variation (3:1) = 2db

FIG. 4-10: HARMONIC RIEKE DIAGRAM

43
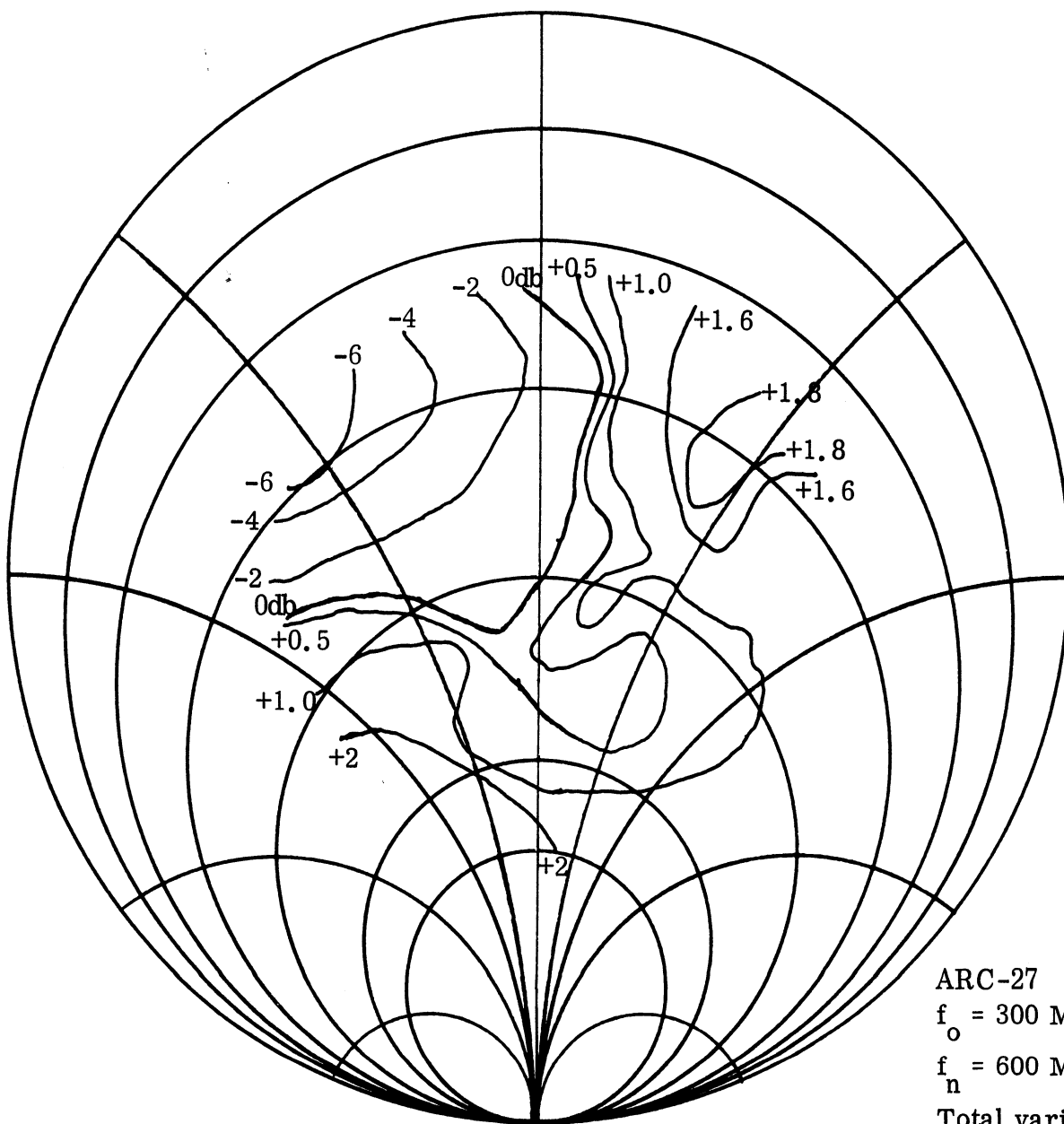
ARC-27   SN-20015
f_o = 300 MHz
f_n = 600 MHz
Total variation (3:1)= 8db

FIG. 4-11: HARMONIC RIEKE DIAGRAM
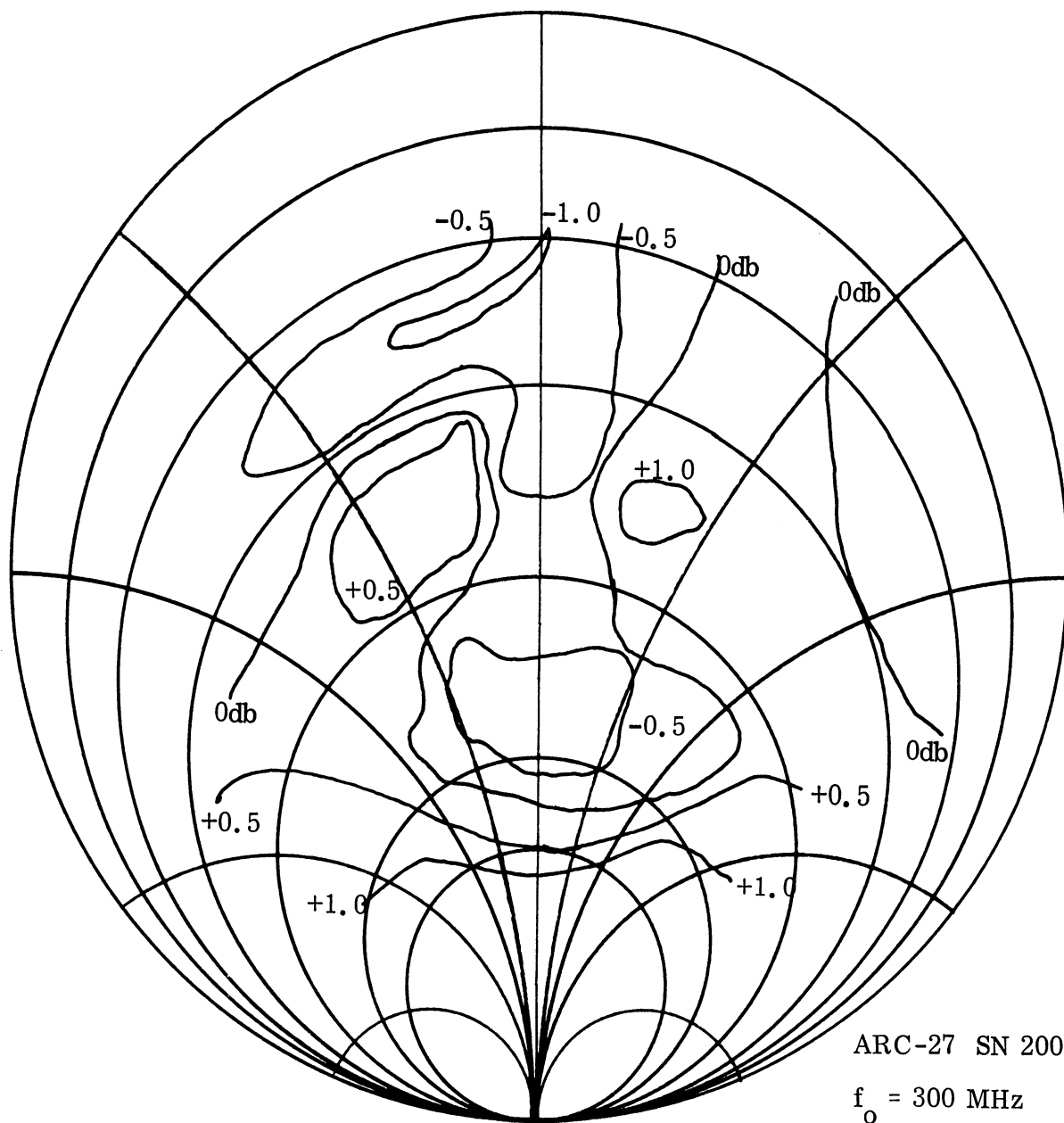
ARC-27 SN 20015

f_o = 300 MHz

f_n = 600 MHz

Total variation (3:1) = 1.5db

FIG. 4-12: HARMONIC RIEKE DIAGRAM

Text within figure:

0db
0db
+1.0
0db
+2
+1
+1.0
+1
0db
0db
-1
-1.0
-2
-2
-3
-3

ARC-27 SN-20015

f_o = 280 MHz

f_n = 560 MHz

Total Variation (3:1) = 3db

FIG. 4-13: HARMONIC RIEKE DIAGRAM
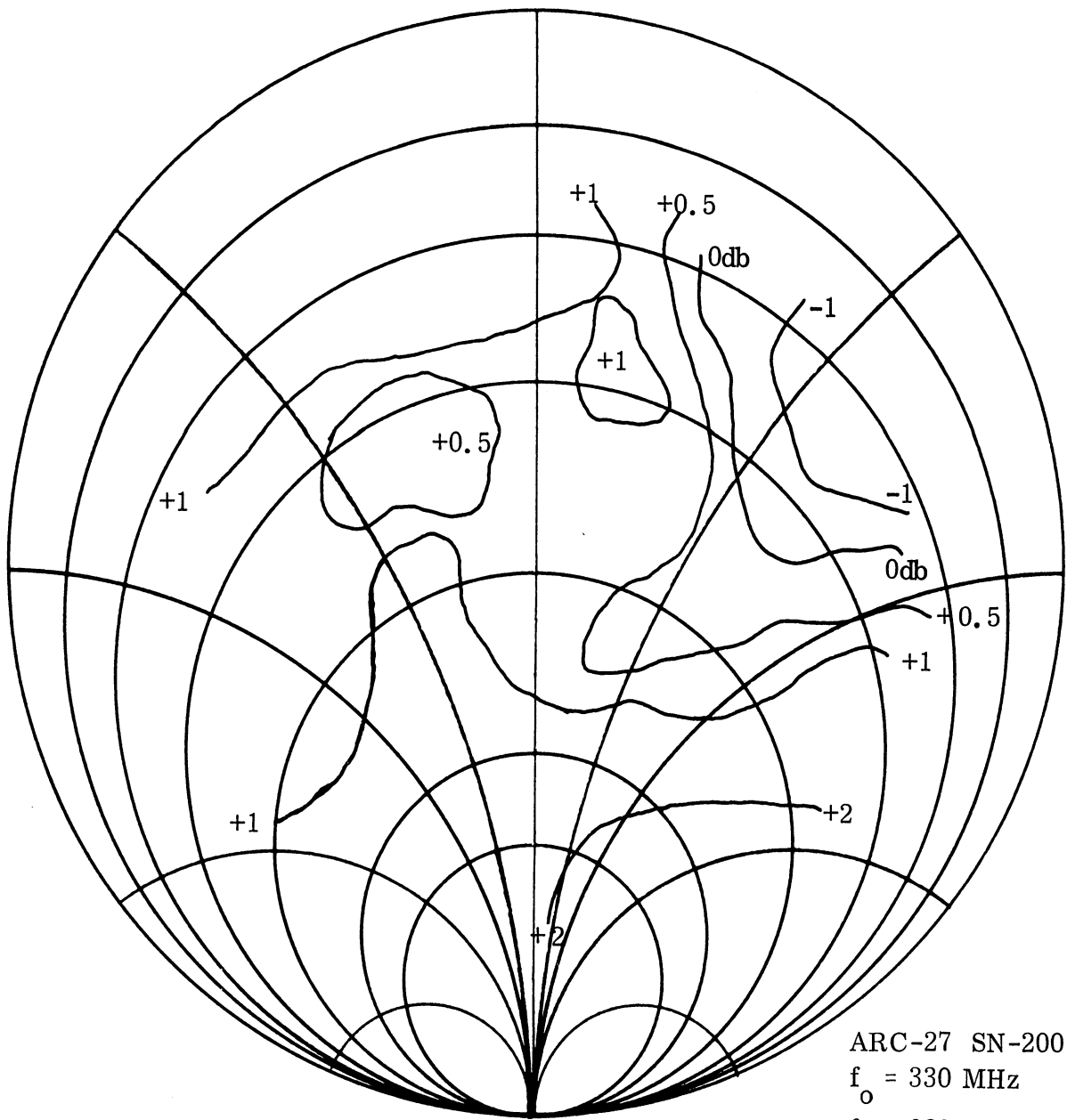
ARC-27 SN-20015
f_o = 330 MHz
f_n = 660 MHz
Total Variation (3:1) = 3db

FIG. 4-14: HARMONIC RIEKE DIAGRAM

ARC-27 SN-20015

f_o = 280 MHz

f_n = 840 MHz

Total Variation (3:1) = 14db

FIG. 4-15: HARMONIC RIEKE DIAGRAM

48

FIG. 4-16: HARMONIC RIEKE DIAGRAM

The diagram is labeled with the following text:
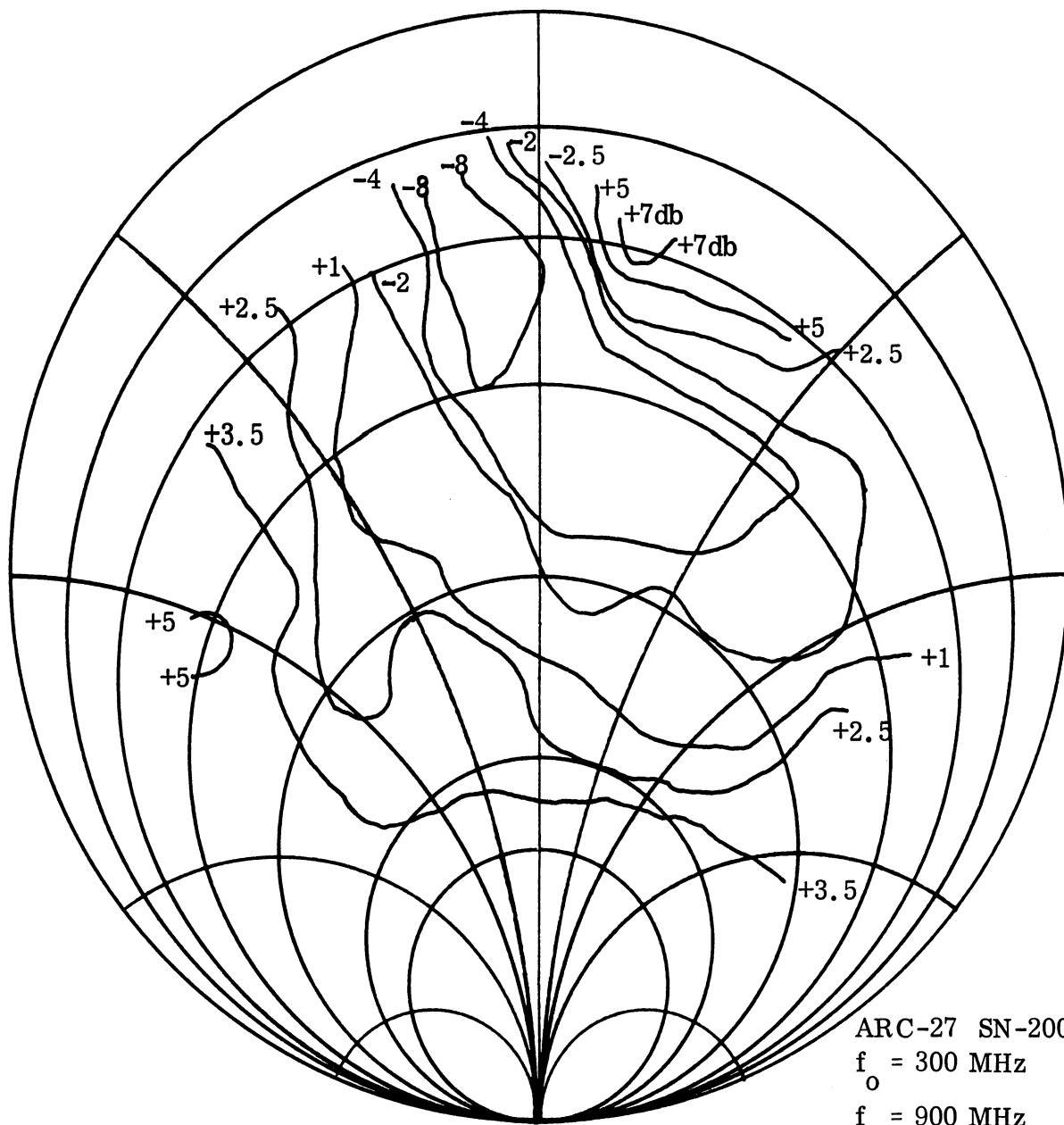
ARC-27 SN-20015

f_o = 300 MHz

f_n = 900 MHz

Total Variation (3:1) = 11.5db
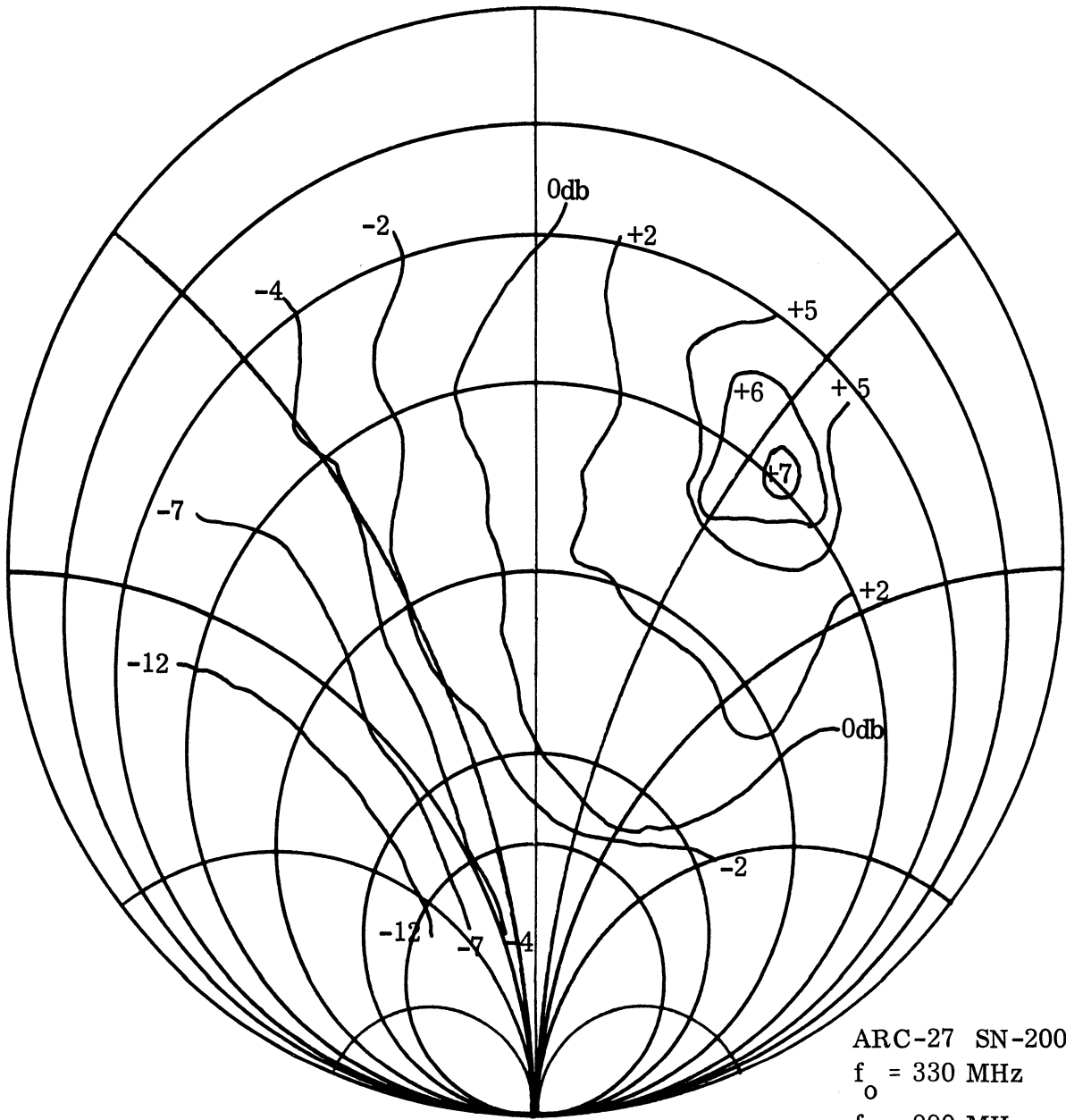
ARC-27 SN-20015

f_o = 330 MHz

f_n = 990 MHz

Total Variation (3:1) = 18db

FIG. 4-17: HARMONIC RIEKE DIAGRAM
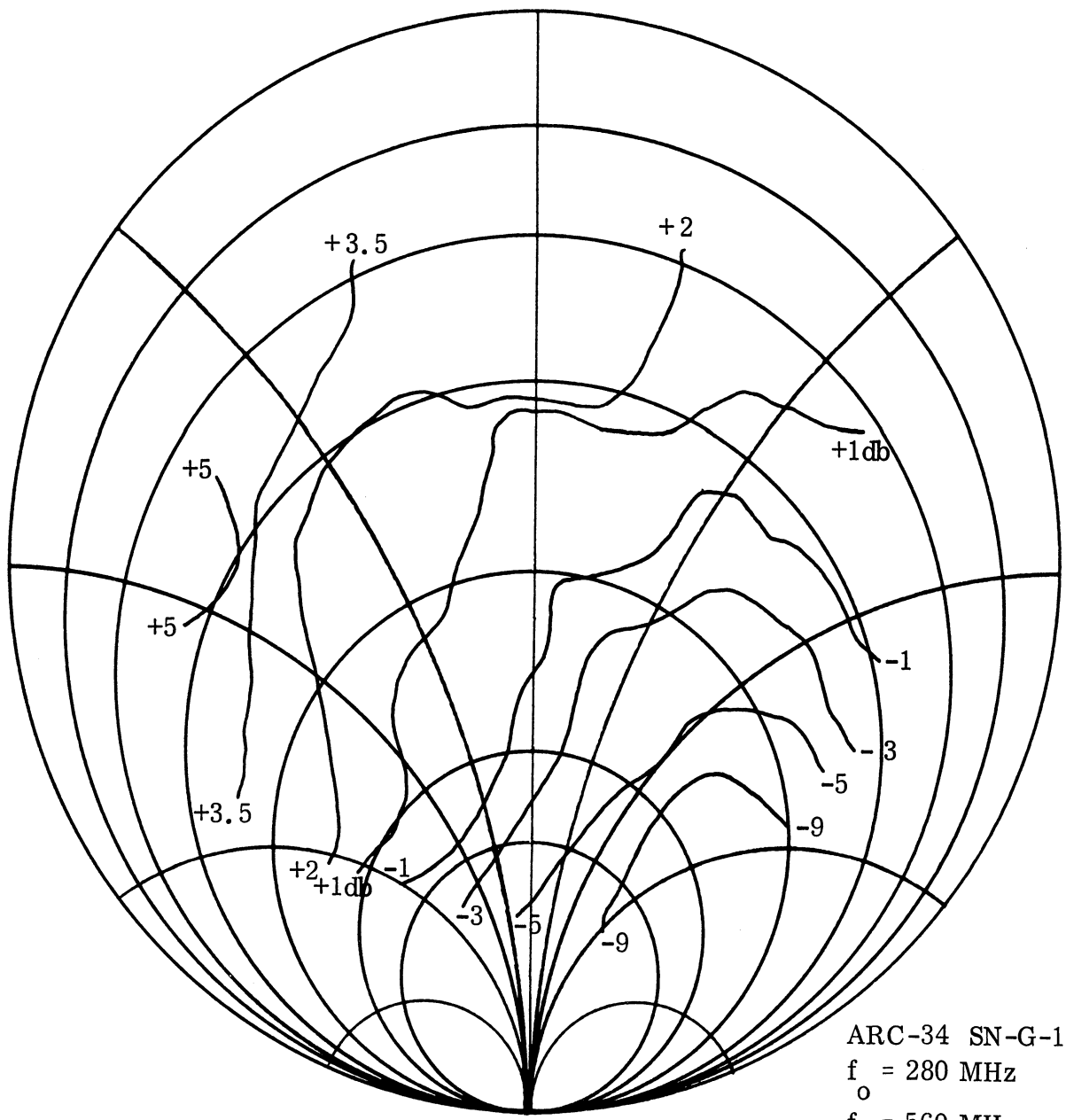
ARC-34 SN-G-12481

f_o = 280 MHz

f_n = 560 MHz

Total Variation (3:1) = 12db

FIG. 4-18: HARMONIC RIEKE DIAGRAM
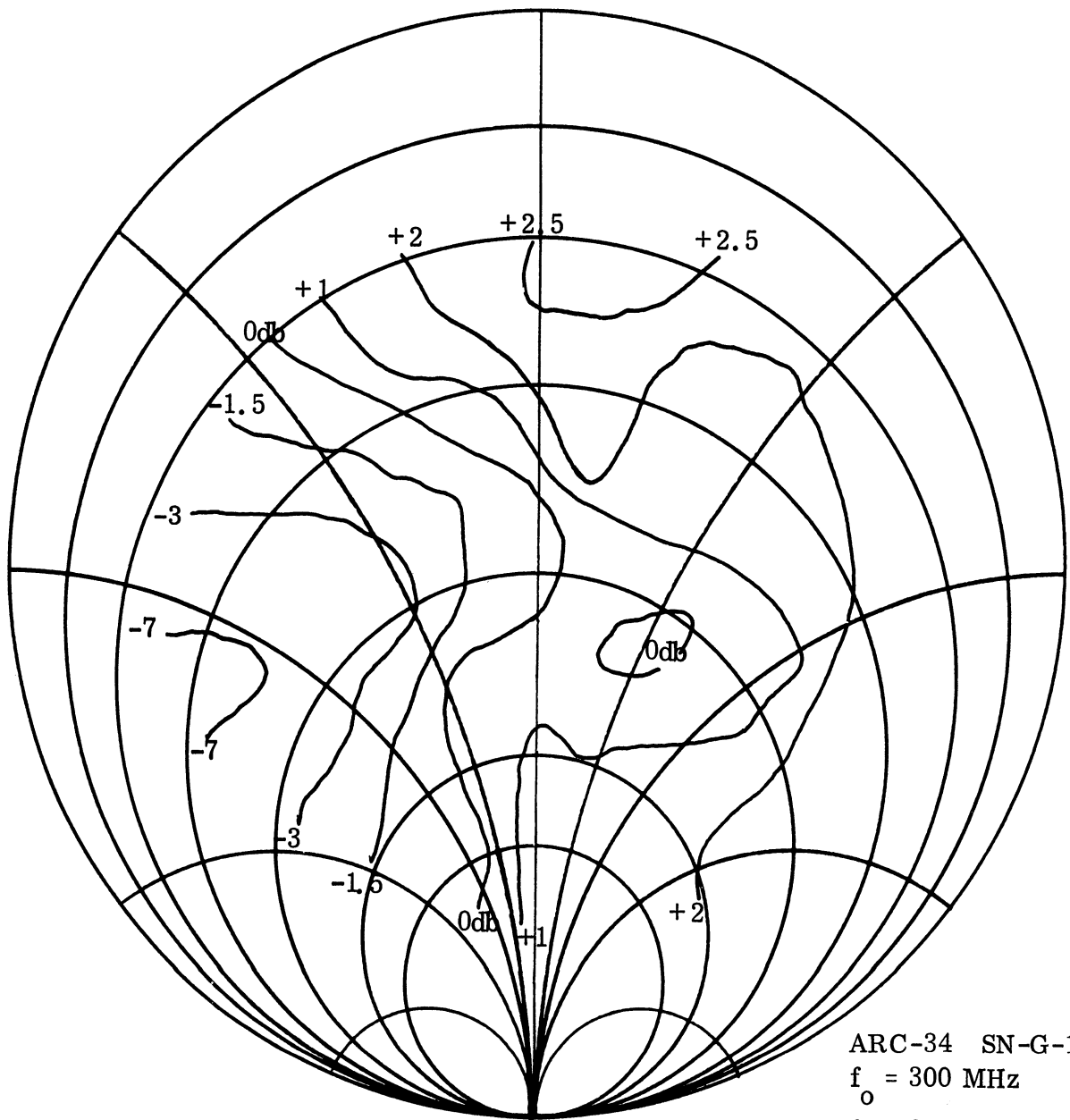
ARC-34   SN-G-12481

$f_o = 300$ MHz

$f_n = 600$ MHz

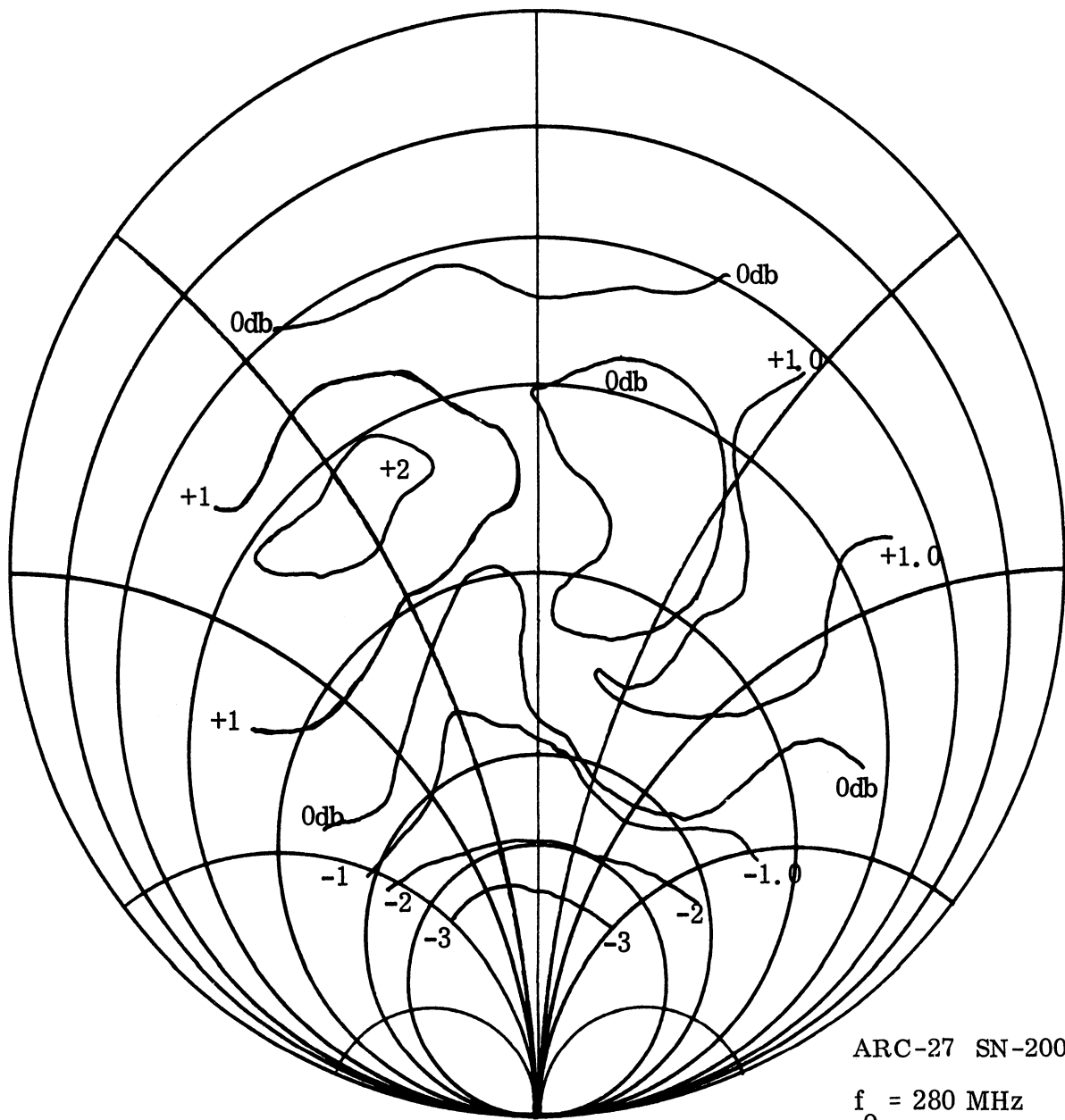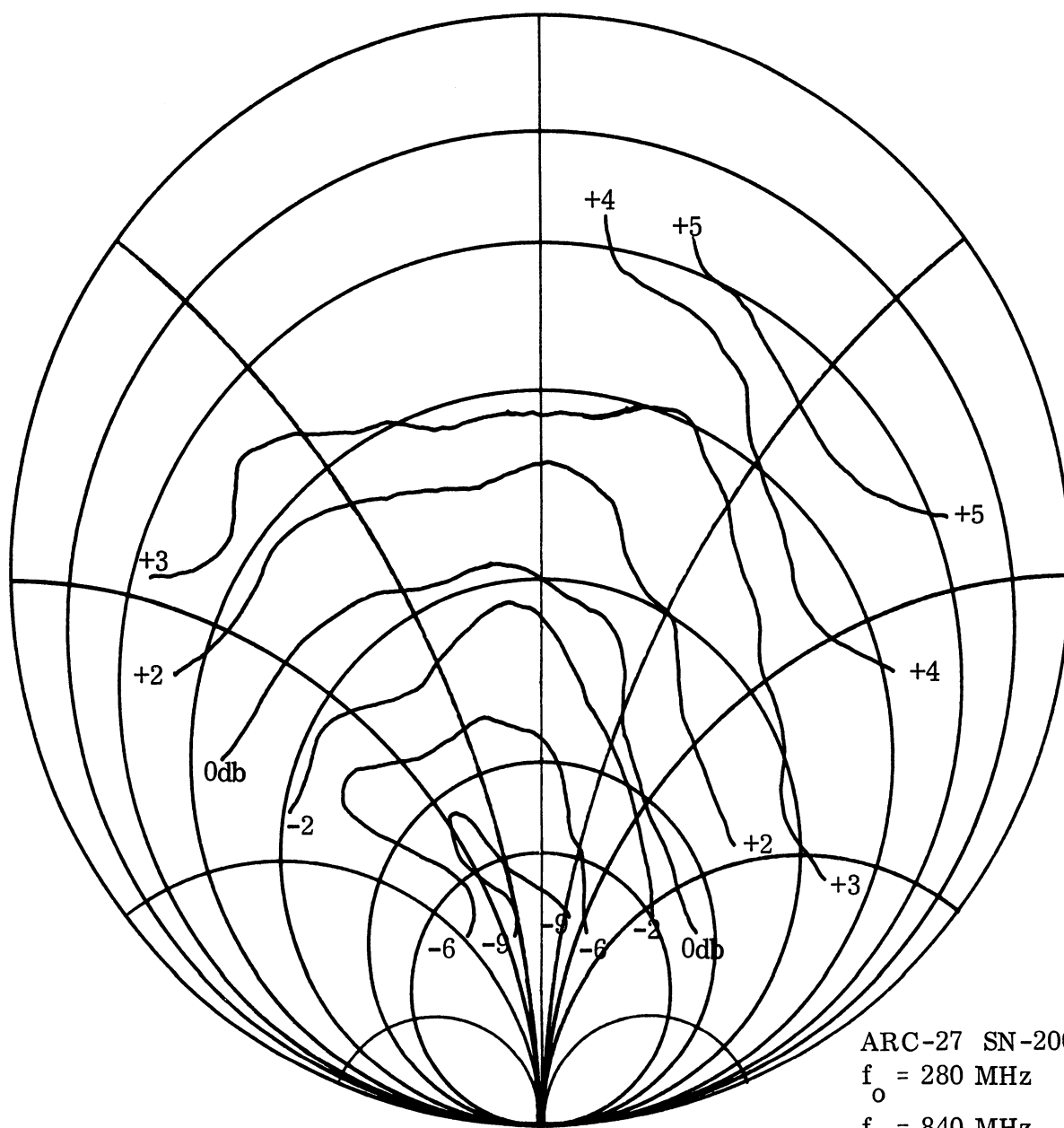Total Variation (3:1) = 7.5 db

FIG. 4-19: HARMONIC RIEKE DIAGRAM

52
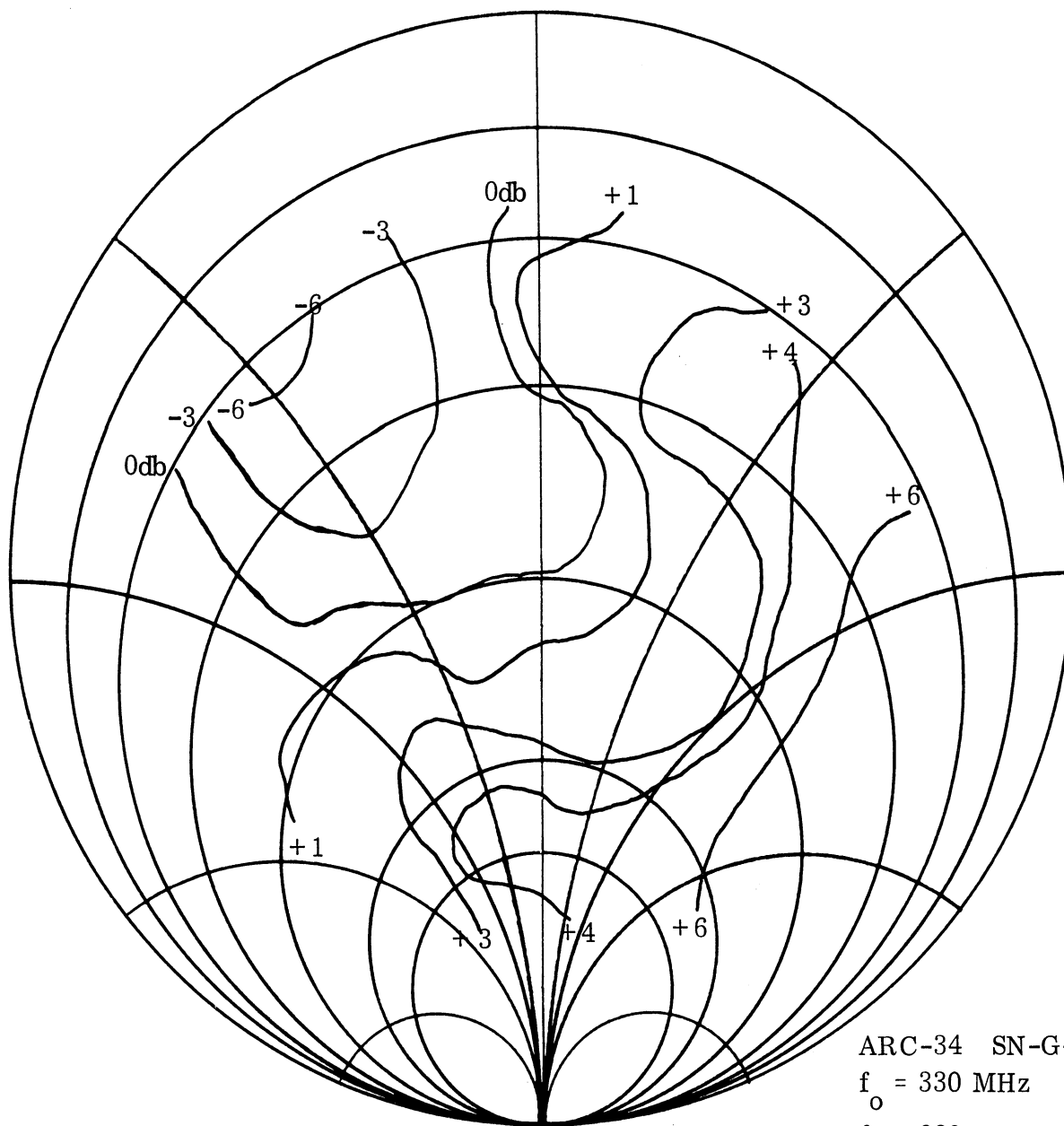
ARC-34 SN-G-12481

f_o = 330 MHz

f_n = 660 MHz

Total Variation (3:1) = 7db

FIG. 4-20: HARMONIC RIEKE DIAGRAM

4.3 Conclusion

The multiple harmonic generator model of Fig. 4-1 predicts no power output variations at frequency f_n with respect to the terminating impedances at the other frequencies. The measurements described in this chapter have shown that the actual behavior is more closely approximated by assuming a constant model superimposed on a model whose output changes with variations in the terminating impedance at the fundamental frequency of operation. It is felt that the variations witnessed are too severe to allow the independent model to provide adequate predictions. The next chapter concerns itself with developing a dependent model to provide a better approximation to the observed behavior.

V

ANALYTICAL TRANSMITTER ANALYSIS

It is clear from the experimental results given in the previous chapter that the model of Fig. 4-1 simply is not adequate for accurate power transfer predictions. We will now attempt to derive a better mathematical model.

5.1   Taylor Series Harmonic Mixer

It has been suggested (Wetherington, Cram and Huntoon, 1964) that a transmitter be represented as a two port device as shown in Fig. 5-1. After attempts to characterize the non-linear device as various configurations of time-varying linear elements, a more general approach was taken. Let us assume only that the output voltage of the non-linear device can be given by a Taylor series expansion of the sum of the two inputs to the device. Further, let us assume that all of the transmitter's harmonic frequencies are terminated in a reflectionless load so that power output variations at the harmonics will be due solely to a non-linear mixing of the fundamental frequency. With these restrictions, the non-linear device is represented as shown in Fig. 5-2.

Expanding the output for the first few terms we have

$$n = 0 \qquad e_o = A_o \qquad\qquad (5.1)$$

$$n = 1 \qquad e_1 = A_1 \left[E_s \cos(\omega t) + E_t \cos(\omega t + \alpha) \right] \qquad (5.2)$$

$$n = 2 \qquad e_2 = A_2 \left\{ \frac{E_s^2}{2} \left[1 + \cos(2\omega t) \right] \right.$$

$$+ \; E_s E_t \left[\cos \alpha + \cos(2\omega t + \alpha) \right]$$

$$\left. + \; \frac{E_t^2}{2} \left[1 + \cos(2\omega t + 2\alpha) \right] \right\} \qquad (5.3)$$
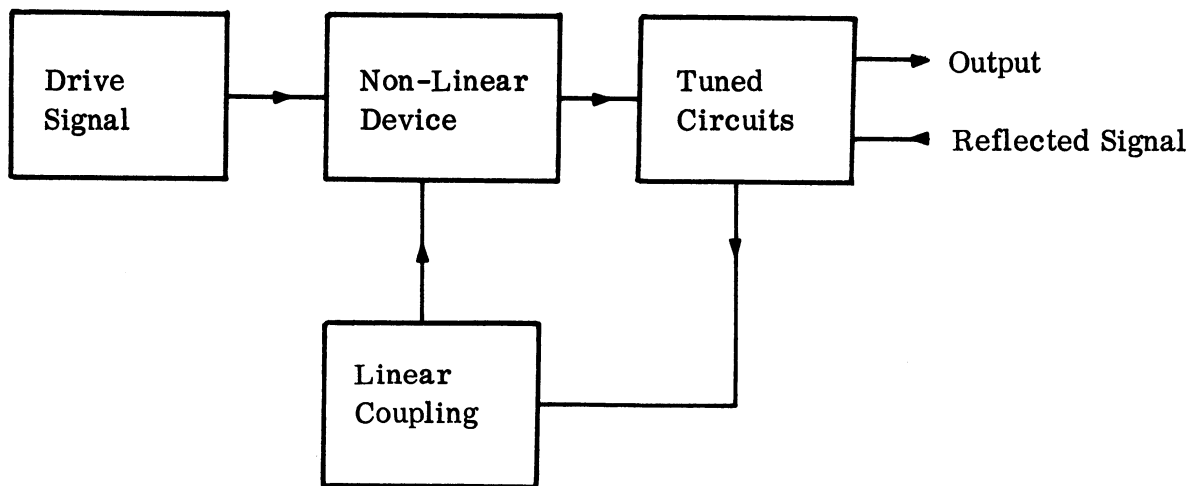
FIG. 5-1: TWO PORT TRANSMITTER REPRESENTATION.

$$E_s \cos \omega t \longrightarrow \bigotimes \longrightarrow \mathcal{E} = \sum_{n=0}^{\infty} e_n = \sum_{n=0}^{\infty} A_n \left[E_s \cos \omega t + E_t \cos(\omega t + \alpha) \right]^n$$

$$E_t \cos(\omega t + \alpha)$$
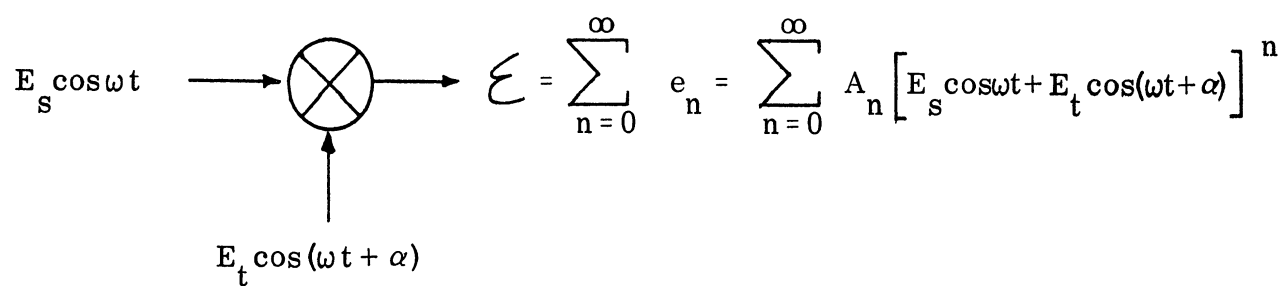
FIG. 5-2: TAYLOR SERIES HARMONIC MIXER

$$n = 3 \qquad e_s = A_3 \left\{ \frac{E_s^3}{4} \left[\cos 3\omega t + 3 \cos \omega t \right] \right.$$

$$+ \frac{3}{4} E_s^2 E_t \left[2 \cos(\omega t + \alpha) + \cos(\omega t - \alpha) + \cos(3\omega t + \alpha) \right]$$

$$+ \frac{3}{4} E_s E_t^2 \left[2 \cos\omega t + \cos(\omega t + 2\alpha) + \cos(3\omega t + 2\alpha) \right]$$

$$\left. + \frac{E_t^3}{4} \left[\cos(3\omega t + 3\alpha) + 3 \cos(\omega t + \alpha) \right] \right\} \qquad (5.4)$$

Combining the terms of argument $2\omega t$ and $3\omega t$ we have a first approximation to the second and third harmonic voltages respectively:

$$H_2 \sim A_2 \left[\frac{E_s^2}{2} \cos 2\omega t + E_s E_t \cos(2\omega t + \alpha) \right.$$

$$\left. + \frac{E_t^2}{2} \cos(2\omega t + 2\alpha) \right] \qquad (5.5)$$

$$H_3 \sim A_3 \left[\frac{E_s^3}{4} \cos 3\omega t + \frac{3}{4} E_s^2 E_t \cos(3\omega t + \alpha) \right.$$

$$\left. + \frac{3}{4} E_s E_t^2 \cos(3\omega t + 2\alpha) + \frac{E_t^3}{4} \cos(3\omega t + 3\alpha) \right] \qquad (5.6)$$

These results have been compared to the variations in harmonic output of an ARC-27 with the harmonics terminated in a reflectionless load while the magnitude and phase of the termination was allowed to vary.

The nature of the variations seems considerably more complex than predicted by (5.5) and (5.6) above. The next section introduces a new method of analysis based more closely on the specific physical design of a real transmitter.

5.2 Spectrum Analysis of an Idealized Class C Amplifier

Thus far the approach to predicting the output behavior of the ARC-27 has been to "imagine" a model and compare the model output characteristics to that of the ARC-27. In this section we will start with a vacuum tube and attempt to model its behavior in a simple amplifier configuration with an eye toward graduating later to the more esoteric systems found in real transmitters.

A simple, general block diagram of a vacuum tube amplifier is found in Fig. 5-3. Restricting ourselves to a specific amplifier we will attempt to analyze the circuit shown in Fig. 5-4.

For the purposes of this analysis we will assume that the passive R, L, C circuit components can be modeled adequately by conventional lumped circuit approximations. It remains to model the vacuum tube. Since we are interested primarily in predicting the spectrum of power amplifiers which are seldom linear, a simple linear controlled source will not suffice. Suppose it is possible to represent the tube by its static characteristics. A possible model appears in Fig. 5-5. $i_b (e_c, e_b)$ is a nonlinear element given by the static characteristics as a function of both the grid and plate voltages. Incorporating this model into the circuit of Fig. 5-4, we have the equivalent amplifier circuit in Fig. 5-6. e_s is the input signal; $Z_s(\omega)$, the impedance of input circuit; $Z_\ell(\omega)$, the impedance of the output; and e_ℓ, the output voltage. E_{cc} and E_{bb} are the grid and plate DC supplies respectively and are assumed to have zero internal impedance. The tube itself is modeled by a controlled current source, the inter-electrode capacitances, and input and output shunt conductances. The value of the current source is a function of the grid and plate voltages, the function being given by a piecewise linear approximation to the device static characteristics. Other types of functions could of course be used to approximate the characteristic curves. A piecewise linear approximation was chosen because it was 1) the simplest to evaluate for a given tube, and 2) led to a more compact solution below. The values of g_g and g_p
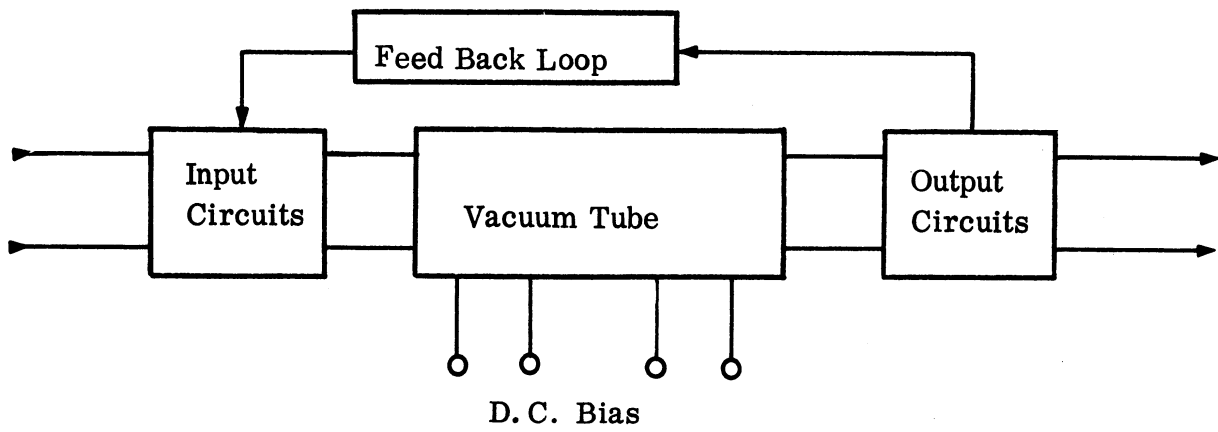
FIG. 5-3: BLOCK DIAGRAM OF A SINGLE STAGE
VACUUM TUBE AMPLIFIER
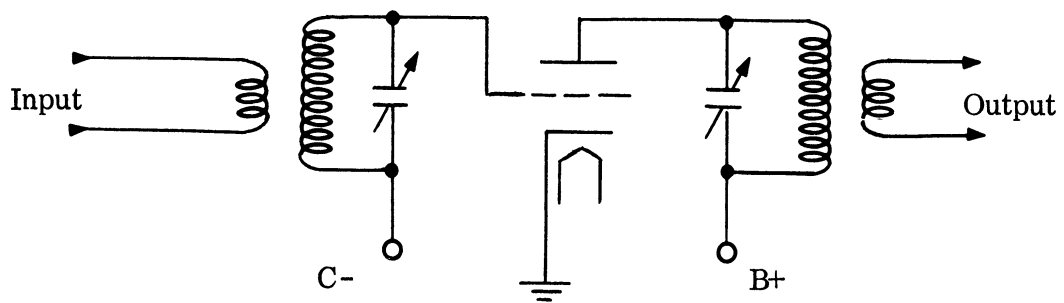
FIG. 5-4: SIMPLE TRIODE AMPLIFIER.
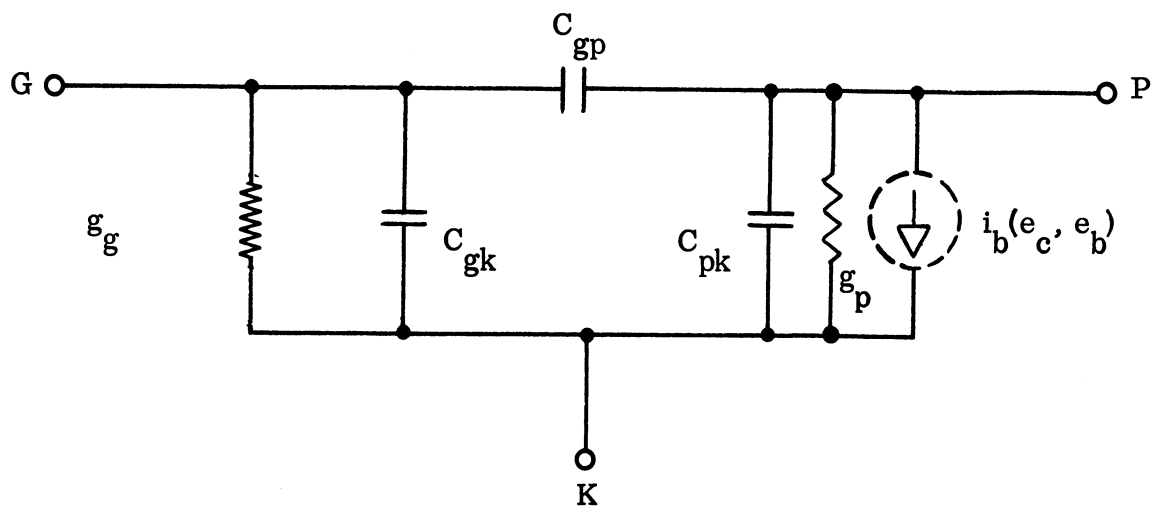
FIG. 5-5: NON-LINEAR MODEL OF A TRIODE.
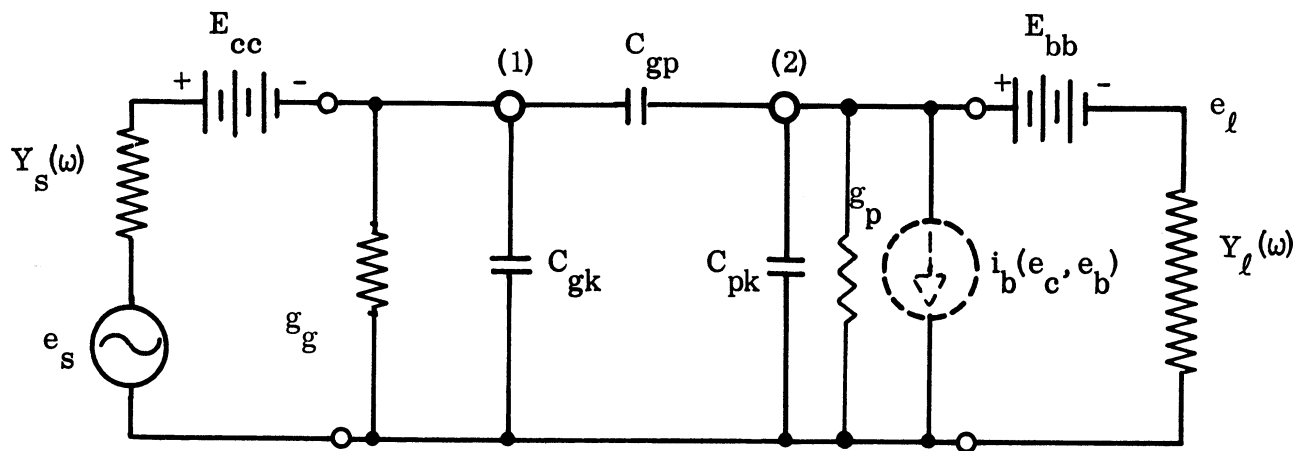
FIG. 5-6: EQUIVALENT CIRCUIT OF A TRIODE AMPLIFIER.

may also be functions of the grid and plate voltages. These variations are neglected in this analysis. The model does not include any attempt to account for lead inductance or electron transit time effects and is therefore frequency limited.

Referring to Fig. 5-6, the frequency domain node voltage equations at nodes (1) and (2) are

$$0 = - \left| E_g \right|_n (n\omega) \left[jn\omega \, C_{gk} + g_g + jn\omega \, C_{gp} + Y_{sn} \, (n\omega) \right]$$

$$+ \left| E_p \right|_n (n\omega) \, jn\omega \, C_{gp} + \left| E_s \right|_n (n\omega) \, Y_{sn} \, (n\omega) - E_{cc} \, Y_{so} \qquad (5.7)$$

and

$$0 = \left| E_g \right|_n (n\omega) \, jn\omega \, C_{gp} - \left| E_p \right|_n (n\omega) \left[jn\omega \, C_{pk} + gp \right.$$

$$\left. + jn\omega \, C_{gp} + Y_{\ell n} \, (n\omega) \right] - I_p \left(E_g, \, E_p \right) + E_{bb} \, Y_{\ell o} \qquad (5.8)$$

Since (5.7) and (5.8) above are written in the frequency domain, there will be a new set of equations for each n, n = 0, 1, 2$\cdots\cdots$. The current, i_b, is specified in the time domain by

$$i_b = A_{r,\,s} \, e_c + B_{r,\,s} \, e_b \qquad (5.9)$$

where A and B are constants chosen appropriately over the regions

$$e_c (r-1) < e_c \leq e_c (r), \qquad e_b (s-1) < e_b \leq e_b (s)$$

to provide the best linear approximation to the tube static characteristics in that region. The shunt conductances g_g and g_p are defined in the conventional manner as

$$g_g = \frac{\partial i_c}{\partial e_c} \qquad (5.10)$$

$$g_p = \frac{\partial i_b}{\partial e_b} \qquad (5.11)$$

Equations (5.7) and (5.8) cannot be simply solved. The equations are in the frequency domain while i_b is known only in the time domain. Since i_b is non-linear in the time domain, it cannot be transformed easily. We will attempt to circumvent these difficulties by approximating i_b and correcting the approximation by an iterative process.

The $\left|E_g\right|_n (n\omega) \, jn\omega \, C_{gp}$ term in (5.8) is the component of current flowing into node 2 through the grid to plate capacitance. This current will normally be small in comparison to the total current at the node. Equation (5.7) can therefore be approximated by

$$I_p (E_g, \ E_p) \simeq E_{bb} \, Y_{\ell o} - \left|E_p\right|_n (n\omega) \left[jn\omega \, C_{pk} \right.$$

$$\left. + g_p + jn\omega \, C_{gp} + Y_{\ell n} (n\omega) \right] \qquad (5.12)$$

A method of solution is diagrammed in Fig. 5-7. The first step is to approximate i_b. Once this approximation has been determined, $i_b(t)$ is transformed to $i_b(\omega)$.

$$i_b (t) = \sum_n \left|\widehat{I_p}\right|_n (n\omega) \qquad (5.13)$$

Substituting the components of i_b given in (5.13) into (5.12) and equating terms of the same frequency, we determine $\left|\widehat{E_p}\right|_n (n\omega)$.

① Approximate $i_b(t)$

② Transform $i_b(t)$ to $I_p(\omega)$

③ Solve (5.8) and (5.12) for $E_p(\omega)$ and $E_g(\omega)$

④ Transform $E_p(\omega)$ and $E_g(\omega)$ to $e_b(t)$ and $e_c(t)$

⑤ Continue to step 6 until e_b is correct

⑥ Solve (5.9) for a better approximation to $i_b(t)$

⑦ Solve (5.20) and (5.21) for the spectrum output
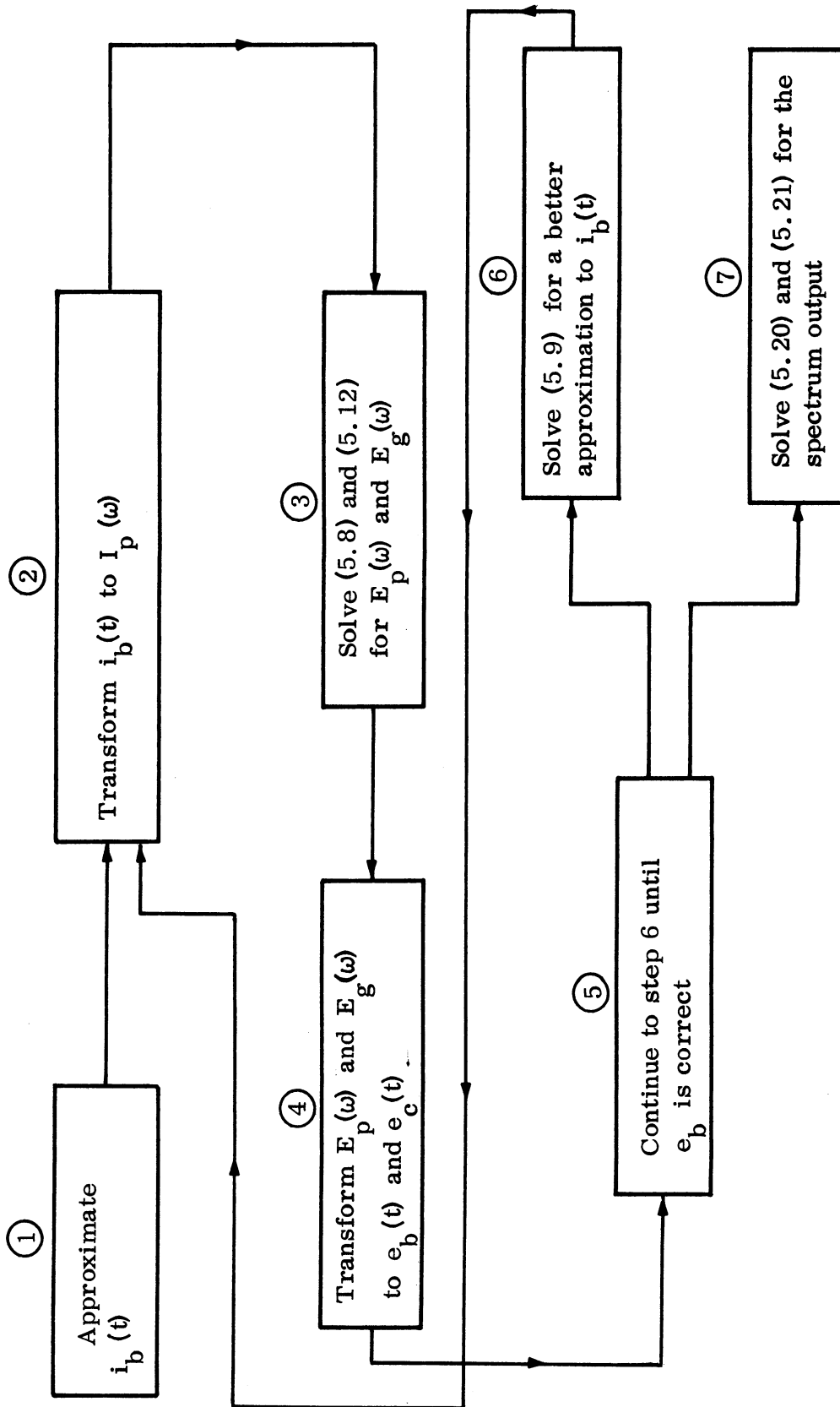
FIG. 5-7: FLOW DIAGRAM FOR THE ITERATIVE SOLUTION.

Once the $E_p\,_n$ $(n\omega)$ have been determined, equation (5.7) can be solved for the grid voltage. The grid and plate voltages are now transformed back into the time domain

$$e_c(t) = \sum_n \left|\widehat{E_g}\right|_n (n\omega)$$
(5.14)

and

$$e_b(t) = \sum_n \left|\widehat{E_p}\right|_n (n\omega)$$
(5.15)

and subsequently substituted into equation (5.9) to obtain better approximations to i_b. This procedure is repeated until e_b has been found to the required degree of precision. At this time the output voltage waveform e_ℓ is given by

$$e_\ell(t) = E_{bb} - e_b(t)$$
(5.16)

The Fourier transform of $e_\ell(t)$ is the load voltage spectrum. The power output spectrum is given by

$$P(n\omega) = \frac{\left|\widehat{E_\ell}\right|_n{}^2 (n\omega)}{2 \, \mathrm{Re}\left[Z_\ell(n\omega)\right]}$$
(5.17)

The foregoing analysis has been applied to a dual tetrode (Amperex 6252). A computer program has been developed to solve the flow diagram in Fig. 5-7. The inputs are the excitation voltage, $e_s(t)$; the DC bias levels; the input and output impedances, $Z_s(\omega)$ and $Z_\ell(\omega)$; and the piecewise linear approximation to the tube characteristics. The outputs are the plate current and load voltage time domain waveforms and the magnitude and phase of the load voltage as a function of the harmonic number. Concurrently, an experimental amplifier was designed around the tetrode and constructed. A diagram of the experimental amplifier appears in Fig. 5-8.

67

The fundamental frequency of operation chosen was 300 MHz because of the availability of an exciter and measurement equipment at that frequency. The experimental equipment arrangement is diagrammed in Fig. 5-9. Several difficulties were encountered at this point. Although the computer analysis was satisfactory, i.e, "reasonable" outputs were obtained for assumed values of input and output impedances; attempts at experimentally determining these parameters have been unsuccessful. Also, if the two cirvuits (Fig. 5-8) are properly balanced, there should be extremely small outputs at the even numbered harmonics. These expectations were accurately reflected by the computer analysis but not obtained experimentally. Lack of time finally precluded further development of the amplifier, forcing abandonment of this approach.

5.3 Discussion of Observed Results

We are thus left with the conclusion that so far no adequate model of the ARC-27 has been devised; the Taylor series approximation was simply inadequate, and time did not allow the completion of the amplifier analysis. This is not to say that one should be discouraged from pursuing either method further; only the first few terms of the power series have been included in the power series analysis. Also, the computer analysis of the amplifier output appears quite promising. Furthermore in the event that the amplifier analysis is deemed too involved to provide results for the general case, it has potential as a design aid to help the designer evaluate the harmonic response of a particular transmitter design.
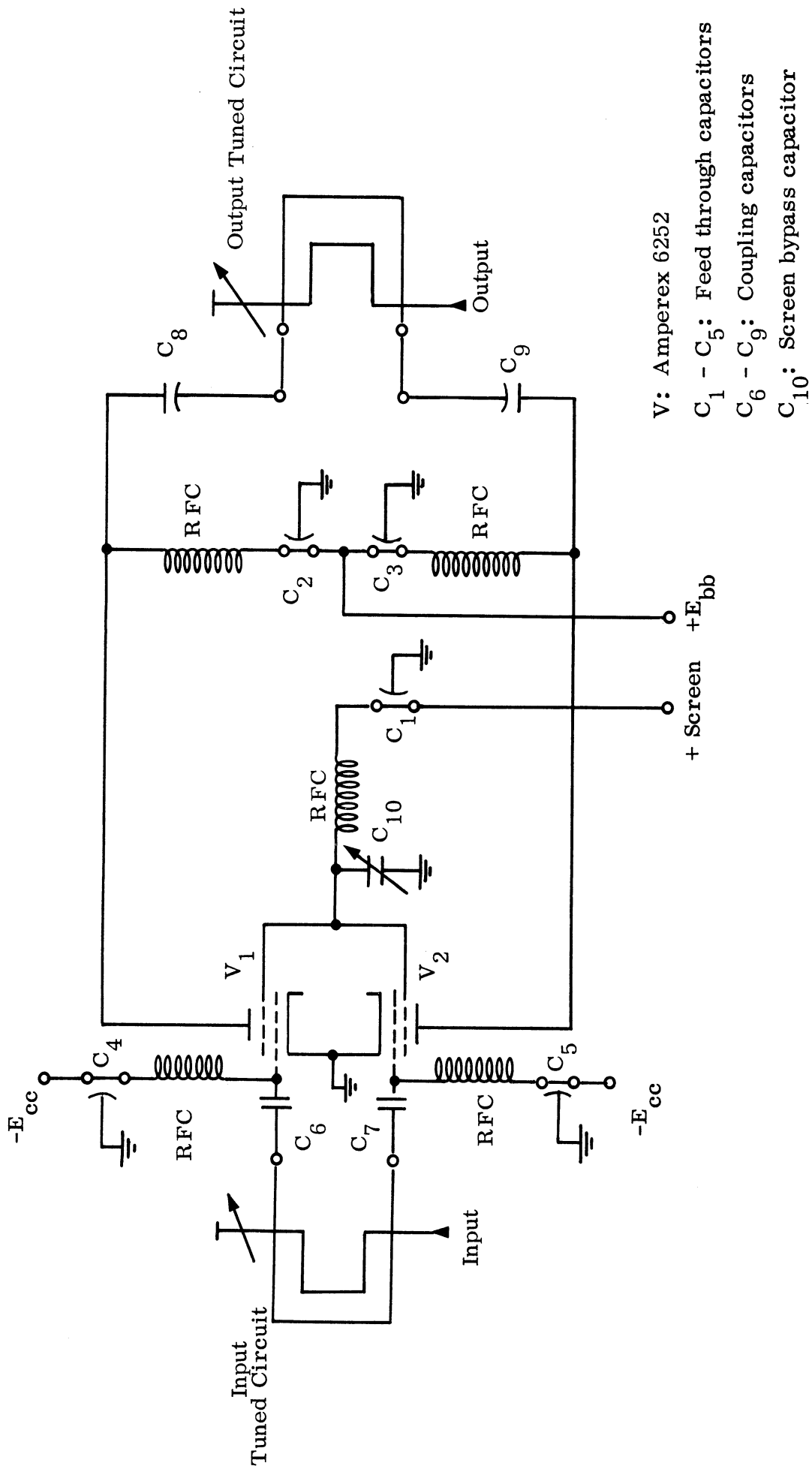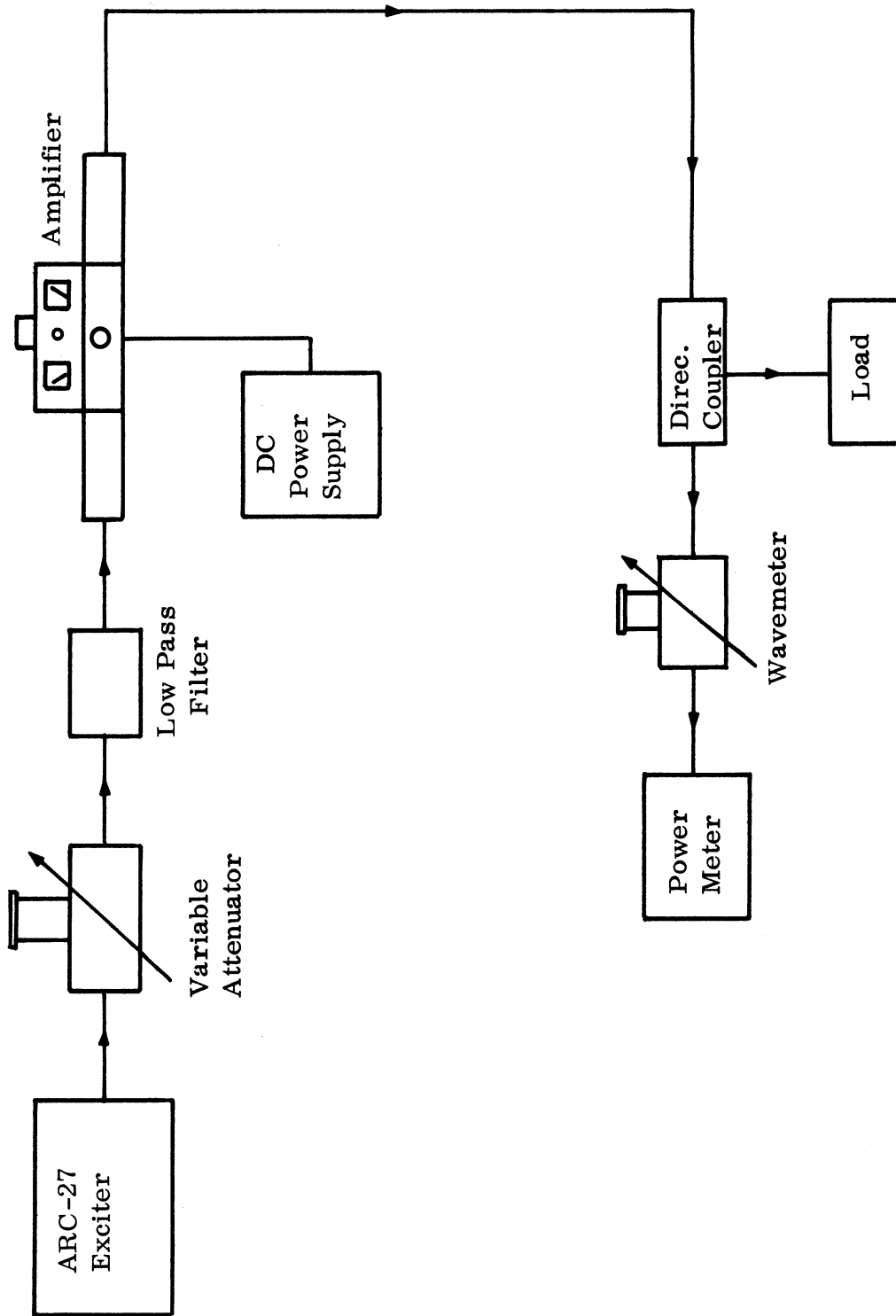
FIG. 5-8: AMPLIFIER SCHEMATIC

V: Amperex 6252

$C_1 - C_5$: Feed through capacitors

$C_6 - C_9$: Coupling capacitors

C_{10}: Screen bypass capacitor

69

FIG. 5-9: BLOCK DIAGRAM OF SPECTRUM SIGNATURE
MEASUREMENT TEST.

VI

CONCLUSIONS

The principal object of this study has been to develop better techniques for obtaining airborne spectrum signatures, the prime payoff being more accurate predictions of the possibility of interference between systems. Toward this end we have attempted to develop mathematical models of airborne radiating systems. The transmission line model described in Chapter II is felt to provide very accurate power transfer results for all but very short sections of high loss transmission lines. An interesting outcome of the transmission line study is that to suppress harmonic radiations, one might choose a transmission line with low loss at the fundamental and higher losses at the harmonic frequencies. Since most transmission lines exhibit this characteristic, it may be possible to minimize spurious and harmonic frequencies through the design of a lossy low pass filter type of transmission line.

The difficulty in applying the transmission line model derived in Chapter II is due to the limited accuracy with which one is able to determine the necessary transmitter parameters. As noted in Chapter II, the derivation of the power transfer model required that the transmitter VSWR and power delivered to a reflectionless load be known. The data presented in Chapter IV reveals that the power delivered to a matched load is a function of the terminating impedance at the fundamental frequency of operation. Further, attempts at analytically describing the functional relationship are incomplete. Therefore, several possibilities remain, e.g., 1) neglect the results presented in this report and assume that the spectral power density delivered to an antenna is the same as that delivered to a matched load; 2) use the transmission line model but assume that the power output does not vary with changes in the load impedance at the fundamental frequency, or 3) collect data similar to the harmonic Rieke diagrams presented in Chapter IV. These data are obtained at each harmonic of interest, for each transmitter at each fundamental frequency of operation. One must then decide what the terminating impedance will be at each fundamental

71

frequency of operation, and use this data along with the power transfer model to compute the spectral energy density delivered to the antenna.

Alternative number one requires the least effort. Errors that may be introduced in the event one neglects to include the transmission line model are typically 1 - 10 db provided the transmitter and antenna VSWR's are less than 10:1 and the line losses are from 2 - 6 db. Additional losses or higher VSWR's will decrease the power transferred. It should be noted that neglecting the transmission line may give an erroneously low answer under conditions of high generator VSWR and low line loss. Neglecting to include the effect of the terminating impedance at the fundamental will cause errors which vary randomly, from typically -10 db to +10 db, at the third harmonic output of an ARC-27 and second harmonic output of an ARC-34. Additional information about other harmonics and transmitter types is not available.

Alternative number two introduces the same errors in transmitter harmonic output power but corrects for the transmission line effects. Therefore, one may reduce the magnitude of the uncertainty of the antenna input power prediction from approximately (-16 db to +10 db) to ($\pm$ 10 db) for the cases cited above. However, the necessary inputs now include transmitter and antenna VSWR's and transmission line loss as a function of frequency as well as the transmitter output spectral energy distribution into a matched load.

The third alternative promises the most accurate predictions but requires several orders of magnitude more effort to collect the required data inputs. Since the harmonic power outputs change from transmitter to transmitter within one transmitter type and even from alignment to alignment within one unit (Figs. 4-11, 4-12) this approach seems feasible only for critical situations involving only a few units.

One of the anticipated outputs from this study was recommendations for changes in Military Standard 449, "Measurement of Radio Frequency Spectrum Characteristics." In view of the discussion given above a change that might well be recommended is to include measurement of the transmitter VSWR at the funda-

mental and harmonic frequencies. The recommended procedure for these measurements is to terminate the fundamental output in a matched load and follow the method described in Section 4.3.2 of Ferris et al (1966). It must be noted, however, that the effects of a mismatch at the fundamental frequency on the transmitter VSWR at harmonic frequencies have not been completely evaluated and more work is recommended in this area.

It must be concluded that the problem of mathematically modeling a real transmitter for the purposes of predicting accurate spectrum signatures is indeed a complex one. It is felt that significant approaches have been indicated and initiated. However, the results are not sufficiently advanced to allow their application to most practical systems without extensive further study.

APPENDIX A

DERIVATION OF CONSTANT POWER CONTOURS
FOR A LINEAR SOURCE ON THE SMITH CHART

The average steady-state power delivered to the load in Fig. A-1, is the real part of the rms voltage appearing across the load multiplied by the complex conjugate of the rms current through the load.

$$P_\ell = \text{Re} \left[E_\ell I_\ell^* \right] \tag{A.1}$$

However, the load will not in general be located directly at the generator terminals. Let the impedance seen by looking into the line in the direction of the load at the plane A A' be Z_a. The average power delivered to Z_a is

$$P_a = R_e \left[E_a I_a^* \right] \tag{A.2}$$

where

$$I_a = \frac{E_g}{Z_g + Z_a} \quad \text{and} \quad E_a = I_a Z_a \tag{A.3}$$

thus

$$E_a = \frac{E_g}{Z_g + Z_a} Z_a \tag{A.4}$$

It is now evident that

$$P_a = \text{Re} \left[\frac{E_g}{Z_g + Z_a} Z_a \cdot \left(\frac{E_g}{Z_g + Z_a} \right)^* \right] \quad \text{or} \tag{A.5}$$

74

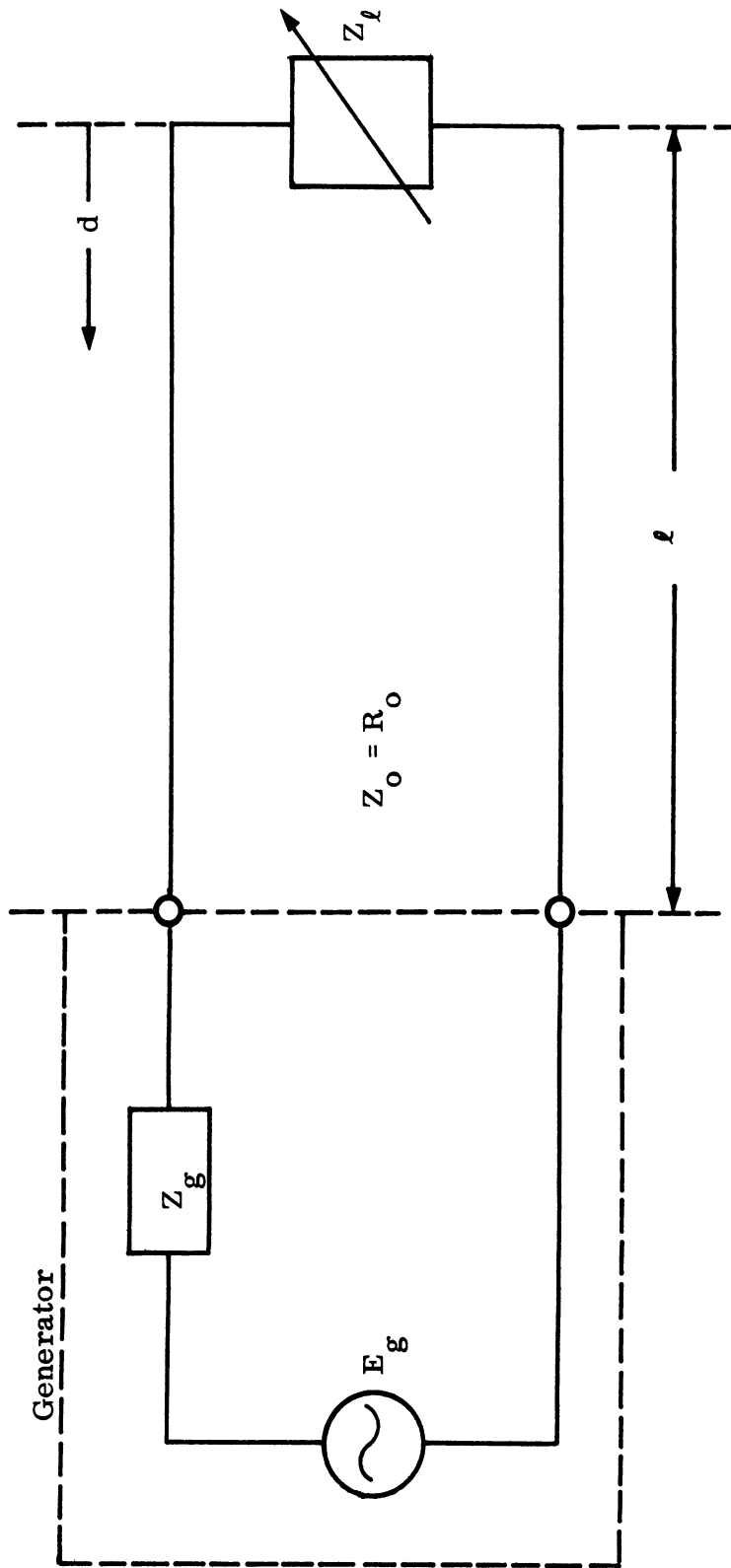FIG. A-1: LOSSLESS POWER TRANSFER MODEL.

$$P_a = \left| \frac{E_g}{Z_g + Z_a} \right|^2 \cdot R_a = \frac{|E_g|^2 R_a}{\left(R_g + R_a\right)^2 + \left(X_g + X_a\right)^2} \qquad * \qquad (A.6)$$

The result, (A.6) may be reduced to a more convenient form. Since it is of interest to plot constant power contours as a function of Z_a, define a constant K_n such that

$$K_n = \frac{|E_g|^2}{P_{a_n}} \qquad (A.7)$$

Combining (A.6) and (A.7),

$$K_n R_a = R_a^2 + 2R_a R_a + R_g^2 + X_a^2 + 2X_n X_g + X_g^2 \qquad (A.8)$$

Rearranging (A.8) and completing the square yields

$$\left[R_a + \frac{2R_g - K_n}{2} \right]^2 + \left[X_a + X_g \right]^2 = \frac{K_n^2 - 4K_n R_g}{4} \qquad (A.9)$$

Equation (A.9) is of the form $U^2 + V^2 = A^2$, implying that Rieke diagrams plotted on a rectangular chart (R_a, abscissa; jX_a, ordinate) and assuming a constant generator internal impedance, will be circles with center at,

$$\left(\frac{K_n}{2} - R_g \right), \quad \left(-X_g \right) \quad \text{and radius} \quad \left[\frac{K_n^2 - 4K_n R_g}{4} \right]^{1/2}.$$

Furthermore, for the radius to be real,

$$K_n^2 \geq 4 K_n R_g \qquad (A.10)$$

---

* Where the complex impedance Z_a has been expressed as $Z_a = (R_a + jXa)$

76

which implies that

$$P_a \leq \frac{\left|E_g\right|^2}{4R_g} \tag{A.11}$$

i.e., the maximum power available to the load can never exceed the square of the generator voltage divided by four times the real part of the generator impedance.

It has been shown that a bilinear transformation of a circle in one complex plane yields a circle in the second (Guillemin, 1949). Thus the circle defined in the Z-plane by equation (A.9) transforms to a circle in the ρ plane, the transformation equation being

$$Z = \frac{1+\rho}{1-\rho} \ . \tag{A.12}$$

Reich, Ordung, Krauss, and Skolnik (1953) have demonstrated that the circle

$$Z = r_o + jx_o + Re^{j\alpha} \tag{A.13}$$

with center at (r_o, jx_o) and radius R in the Z-plane transforms to the circle,

$$Z = \left|\rho_o\right| e^{j\beta}o + R_\rho e^{j\alpha}\rho \tag{A.14}$$

in the ρ plane. In terms of the parameters of (A.13),

$$R_\rho = \frac{2R}{(r_o + 1)^2 + x_o^2 - R^2} \tag{A.15}$$

$$\left|\rho_o\right| = \left\{ \left[\frac{(r_o-1)^2 + x_o^2 - R^2}{(r_o+1)^2 + x_o^2 - R^2} \right]^2 + \left[\frac{-2x_o}{(r_o+1)^2 + x_o^2 - R^2} \right]^2 \right\}^{1/2} \tag{A.16}$$

$$\beta_o = \tan^{-1} \left(\frac{-2x_o}{r_o^2 - 1 + x_o^2 - R^2} \right) \qquad (A.17)$$

Substituting

$$r_o = \frac{K_n - 2R_g}{2}, \quad x_o = -X_g, \quad \text{and} \quad R = \left[\frac{K_n^2 - 4K_n R_g}{4} \right]^{1/2} \qquad (A.18)$$

from (A.9) into (A.15), (A.16), and (A.17)

$$R_\rho = \frac{\left[K_n^2 - 4K_n R_g \right]^{1/2}}{(R_g - 1)^2 + K_n + X_g^2} \qquad (A.19)$$

$$\rho_o = \frac{\left[R_g^2 + X_g^2 - 1^2 + 4X_g^2 \right]^{1/2}}{(R_g - 1)^2 + K_n + X_g^2} \qquad)A.20)$$

$$\beta_o = \tan^{-1} \left(\frac{-2X_g}{R_g^2 + X_g^2 - 1} \right) \qquad (A.21)$$

Once the parameters of (A.9) have been determined, the constant power contours can be mapped directly onto a Smith Chart as the circle (A.14) with center at $\left(|\rho_o|, \beta_o \right)$ and radius R_ρ.

Figure A-2 is a plot of (A.9) on the Smith Chart, for case $Z_g = 1.5 - j0.5$ (normalized). Notice that the loci of the centers of the circles form a straight line corresponding to a constant angle of reflection coefficient.
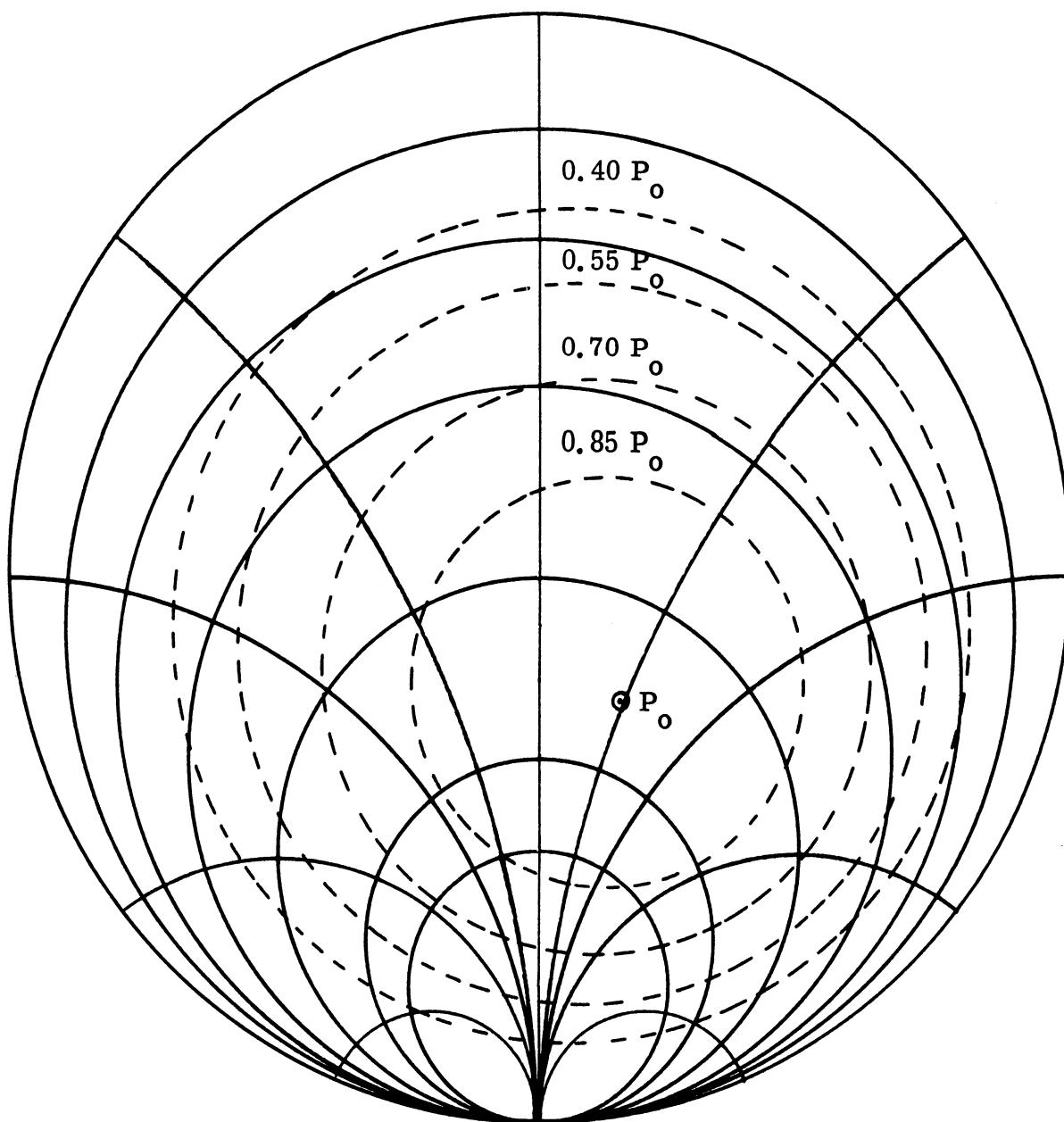
FIG. A-2: THEORETICAL RIEKE DIAGRAM: $Z_g/Z_o = 1.5 - j0.5$

REFERENCES

Cruft Laboratory (1947), Electronic Circuits and Tubes, McGraw-Hill, Inc., New York, N. Y., pp. 423-462.

DeHart, Wilbur R. (1966) "Transmitter to Antenna Power Transfer under Unmatched Conditions," IEEE Trans. on EM Compatibility, June 1966, EMC-8, No. 2, pp. 74-80.

Eaves, J. L., Z. A. Huntoon, and R. D. Wetherington (1963), "A Study of Receiver and Transmitter Non-Linearities," Technical Memorandum X003-19, Electromagnetic Compatibility Analysis Center, Annapolis, Maryland, October 1963.

Ferris, J. E., et al (1966), "Investigation of Measurement Techniques for Obtaining Airborne Antenna Spectrum Signatures," Final Report AFAL-TR-66-101, July, 1966, University of Michigan Radiation Laboratory Report 7274-1-F.

Guillemin, E. A. (1949), The Mathematics of Circuit Analysis, John Wiley and Sons, Inc., 1949. pp. 360-373.

Potter, James L. and Sylvan Fitch (1963), Theory of Networks and Lines, Prentice-Hall, Englewood Cliffs, New Jersey, 1963. Chapters 8 and 9.

Reich, H. J., Philip Ordung, Herbert Krauss, and John G. Skolnik (1953), Microwave Theory and Techniques, D. VanNostrand Co., Inc., Princeton, N. J., 1953, pp 856-862.

Scherer, Jacob, W. Duff and K. Heisler (1966), "Compatibility Prediction Accuracy as a Function of Spectrum Signature Data Inputs," IEEE Electromagnetic Symposium Digest, July 1966.

Tucker, D. G. (1964), Circuits with Periodically Varying Parameters, D. VanNostrand Co., Inc., Princeton, N. J., 1964, Chapter 2.

Very High Frequency Techniques, Radio Research Laboratory, Harvard University, Boston Technical Publishers, Inc., Cambridge, Mass. 1965.

Wetherington, R. D., M. E. Cram and Z. A. Huntoon (1964), "Radio Frequency Intermodulation", Electromagnetic Compatibility Analysis Center Technical Memorandum No. TM X003-26, AD 451416.

DOCUMENT CONTROL DATA - R & D

(Security classification of title, body of abstract and indexing annotation must be entered when the overall report is classified)

1. ORIGINATING ACTIVITY *(Corporate author)*	2a. REPORT SECURITY CLASSIFICATION
The University of Michigan Radiation Laboratory, Dept. of Electrical Engineering, 201 Catherine Street, Ann Arbor, Michigan 48108	UNCLASSIFIED
	2b. GROUP

3. REPORT TITLE

TRANSMITTER IMPEDANCE CHARACTERISTICS FOR AIRBORNE SPECTRUM SIGNATURE

4. DESCRIPTIVE NOTES *(Type of report and inclusive dates)*
Final Report (April 1966 - January 1968)

5. AUTHOR(S) *(First name, middle initial, last name)*

William B. Henry,   Wilbur R. DeHart,   Joseph E. Ferris

6. REPORT DATE	7a. TOTAL NO. OF PAGES	7b. NO. OF REFS
June 1968	81	11

8a. CONTRACT OR GRANT NO.	9a. ORIGINATOR'S REPORT NUMBER(S)
AF 33(615)-3454	
b. PROJECT NO.	7956-1-F
4537	
c.	9b. OTHER REPORT NO(S) *(Any other numbers that may be assigned this report)*
d.	AFAL-TR-68-56

10. DISTRIBUTION STATEMENT
This document is subject to special export controls and each transmittal to foreign governments or foreign nationals may be made only with prior approval of AFAL(AVWE) Wright-Patterson AFB, Ohio 45433.

11. SUPPLEMENTARY NOTES	12. SPONSORING MILITARY ACTIVITY
	Air Force Avionics Laboratory, AVWE Wright-Patterson AFB, Ohio 45433

13. ABSTRACT

The problem of predicting airborne spectrum signatures is divided into three sections: 1) the transmitter spectrum signatures, 2) the effect of the transmission line, and 3) the radiation characteristics of the antenna and airframe. This report is concerned with the first two of these sections, the third having been studied on a predecessor contract (Ferris et al, 1966). Transmission lines are studied first. Expressions for the power transfer through a lossy transmission line as a function of line length, loss, and antenna and transmitter VSWR are developed. The results are valid for single mode systems.

After developing the power transfer expressions, the transmitter behavior is studied. It has been found that the level of the harmonics generated is somehow related to the impedance of the termination at the fundamental frequency. These results are presented graphically in the form of "harmonic" Rieke diagrams. Finally, models to predict this behavior are introduced. No adequate model has been developed but neither has the last proposed model been discarded. More work in this area is indicated before a transmitter behavior can be accurately predicted.

DD FORM 1 NOV 65 **1473**

14. KEY WORDS	LINK A		LINK B		LINK C	
	ROLE	WT	ROLE	WT	ROLE	WT
Electromagnetic Compatibility						
Interference						
Harmonic Frequency						
Transmitter Impedance						
Antenna Patterns						